NASA TECHNICAL NOTE

NASA TN D-4539

C. 1

NASA TN D-4539

A METHOD FOR PREDICTING SHOCK SHAPES AND PRESSURE DISTRIBUTIONS FOR A WIDE VARIETY OF BLUNT BODIES AT ZERO ANGLE OF ATTACK

by George E. Kaattari

Ames Research Center
Moffett Field, Calif.

NATIONAL AERONAUTICS AND SPACE ADMINISTRATION • WASHINGTON, D. C. • APRIL 1968

NASA TN D-4539

A METHOD FOR PREDICTING SHOCK SHAPES AND PRESSURE DISTRIBUTIONS FOR A WIDE VARIETY OF BLUNT BODIES AT ZERO ANGLE OF ATTACK

By George E. Kaattari

Ames Research Center
Moffett Field, Calif.

NATIONAL AERONAUTICS AND SPACE ADMINISTRATION

For sale by the Clearinghouse for Federal Scientific and Technical Information
Springfield, Virginia 22151 – CFSTI price $3.00

A METHOD FOR PREDICTING SHOCK SHAPES AND PRESSURE DISTRIBUTIONS FOR A WIDE VARIETY OF BLUNT BODIES AT ZERO ANGLE OF ATTACK

By George E. Kaattari

Ames Research Center

SUMMARY

A method is presented for determining shock envelopes and pressure distributions for a variety of blunt bodies at zero angle of attack. Correlation functions obtained from exact solutions are used to relate the shock standoff distance, at the stagnation and sonic points, to the body geometry. These functions were obtained for a perfect gas but may be applied for real gases in equilibrium flows. The method is restricted to cases where the bow shock is detached from the body and the flow over the forward face is subsonic. Results given by the method are shown to be in good agreement with experimental values.

INTRODUCTION

A problem currently receiving wide attention is that of predicting the shock envelope and pressure distribution over the forward face of axisymmetric blunt bodies at atmospheric entry.

Exact solutions have been presented for spheres, ellipsoids, and paraboloids by Van Dyke (ref. 1). In this work and that of subsequent investigators most exact solutions are for the indirect problem; a shock shape is prescribed and the resultant body shape is sought. Many trial solutions are usually necessary to find a body shape that approximates the one for which a solution is wanted.

An approximate "direct" method to define the shock trace at zero angle of attack is included in the analysis of reference 2. This method is restricted to spherically blunted bodies with sharp corners. Extensions of this method which permit the calculation of the entire forward shock envelope and the pressure distribution for these bodies have been published (refs. 3 and 4). The exact and approximate solutions of these references are applicable to a relatively narrow choice in body shape.

This investigation was undertaken to develop methods for predicting the shock envelopes and pressure distributions over the forward face of a wide variety of body shapes at zero angle of attack. Particular attention is given to ellipsoids (ranging from a sphere to a flat disk), spherical or

flat-faced bodies with an arbitrary degree of corner rounding, and spherically blunted, large-apex-angle cones. The method developed is restricted to those cases in which the bow shock is detached from the body and the flow over the forward face of the body is subsonic.

NOTATION

A	coefficient in transformed pressure distribution function
a	semiminor axis of ellipsoid
B_b	body bluntness parameter, $y^2 = 2R_b x_b - B_b x_b^2$ (ref. 1)
B_s	shock bluntness parameter, $y^2 = 2R_s x_s - B_s x_s^2$ (ref. 1)
b	semimajor axis of ellipsoid
C	coefficient in transformed pressure distribution function
G	shock correlation function (see eqs. (1))
M	free-stream Mach number
m'_{st}	slope of transformed pressure distribution function at stagnation point
m'_*	slope of transformed pressure distribution function at sonic point
p	pressure on body
p_{st}	pressure at stagnation point on body
p_*	pressure at sonic point on body
R_b	body surface radius on axis of symmetry
R_{b*}	body surface radius at sonic point of an ellipsoid
$R_{b\Phi}$	body surface radius at point on surface inclined Φ degrees with respect to a plane normal to free-stream direction
R_s	shock radius on axis of symmetry
r_c	corner radius of body
r_m	semidiameter of body
s	distance along body surface from stagnation point

s_* distance along body surface from stagnation point to sonic point on body

s'/s'_* independent variable for transformed pressure distribution function

s'_t/s'_* tangent point of transformed pressure distribution functions

V_1 free-stream velocity

V_* velocity at sonic point on body

x_b streamwise distance from apex of body to sonic point on body

x_s streamwise distance from apex of shock to point on shock at distance y_* from axis of symmetry

y normal distance from axis of symmetry

y_* normal distance from axis of symmetry to sonic point on body

Z coordinate axis of transformed pressure distribution function

z dependent variable in transformed pressure distribution function

γ specific heat ratio

Δ shock standoff distance from body in free-stream direction

Δ_o shock standoff distance from body on axis of symmetry in free-stream direction

Δ_* shock standoff distance from sonic point on body in free-stream direction

ϵ inclination on forward body surface at the tangent point with corner radius, r_c

η normal distance from body surface (sketch (g))

θ shock surface inclination at distance, y, from axis of symmetry with respect to plane normal to free-stream direction

θ_* shock surface inclination at a point opposite the sonic point on the body with respect to a plane normal to the free-stream direction

θ_{*o} shock surface inclination, at a point opposite the sonic corner of a flat disk, with respect to a plane normal to the free-stream direction

ν pressure correlation function

ρ_1 density of free stream

ρ_2 density of stream behind normal shock

ρ_{st} density of gas at stagnation point

σ shock layer thickness normal to body (sketch (g))

Φ body surface inclination with respect to plane normal to free-stream direction

Φ_* body surface inclination at sonic point with respect to plane normal to free-stream direction

Φ_{*1} body surface inclination of a sphere at the sonic point with respect to a plane normal to the free-stream direction

ANALYSIS

The analysis will be developed in three parts. First, general relationships and assumptions involving body and shock geometry are introduced. Next, application of the shock-body relationships to a method for calculating the shock envelopes of a variety of blunt bodies is demonstrated. The calculation involved is simplified by the use of a nomograph. Finally, a general method for estimating the pressure distribution for the bodies considered is presented.

General Shock-Body Relationships

Shock shape.- Reference 1 defined shock traces as conic sections of suitable bluntness B_s (see Notation) to obtain the shock solution for a range of conic section blunt bodies. In the present investigation, it was assumed that conic sections can closely approximate the shock trace for a larger variety of blunt bodies than were considered in reference 1.

Stagnation-point correlation.- A relationship involving shock standoff distance, shock shape, and normal-shock density ratio was pointed out in reference 5 and used in reference 2. A simplified form of this correlation, as used in the present investigation, is

$$G = \left(1 + \frac{\Delta_o}{R_b}\right)\frac{\Delta_o}{R_s} = \left(1 + \frac{R_s\Delta_o}{R_b R_s}\right)\frac{\Delta_o}{R_s} \tag{1a}$$

$$\frac{\Delta_o}{R_s} = \frac{\sqrt{1 + 4G\left(\frac{R_s}{R_b}\right)} - 1}{2\left(\frac{R_s}{R_b}\right)} \tag{1b}$$

G is a function of the free-stream gas and Mach number and was evaluated by substituting values for Δ_o/R_s and Δ_o/R_b from reference 1 into equation (1a). Figure 1 shows G as a function of the reciprocal normal-shock density ratio ρ_1/ρ_2 (rather than Mach number) for two values of the gas specific heat ratio, γ.

Sonic point shock standoff correlation.- The theoretical results of reference 1 and numerous experimental results for a variety of body shapes indicate that the ratio, Δ_*/y_*, is primarily a function of the normal-shock density ratio and secondarily of γ pertinent to the free-stream gas in question. Sketch (a) shows Δ_*, the shock thickness measured in the free-stream direction from the sonic point on the body at y_*, the vertical distance from the axis of symmetry.

A correlation of both theoretical and experimental values of Δ_*/y_* with the normal-shock density ratio, ρ_1/ρ_2, is shown in figure 2. The dashed extension of the $\gamma = 1.4$ line is physically unreal, but it is a useful interpolation guide for Δ_*/y_* at values of γ between 1.0 and 1.4.

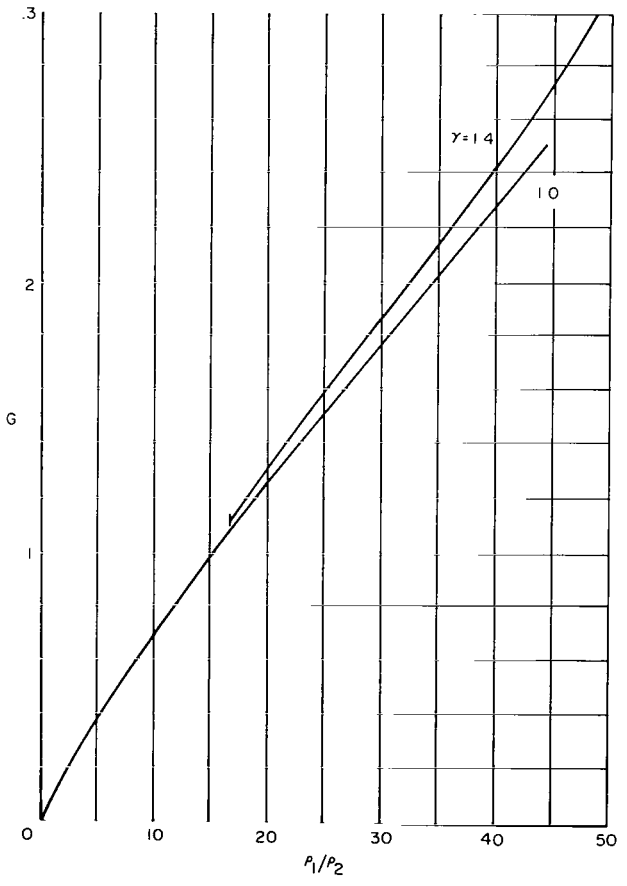

Figure 1.- The G function.

Sonic point inclination.- A solution for the infinite shock-density ratio was used to determine the inclination of the sonic point on conic-section bodies. The results were then applied to finite shock-density ratios and to bodies of other shapes.

The angle, Φ_*, associated with the sonic point is the angle between a normal to the free-stream direction and a line tangent to the body at the sonic point (sketch (a)). This angle was determined with the Busemann solution for an infinite shock-density ratio as a function of the body bluntness parameter,

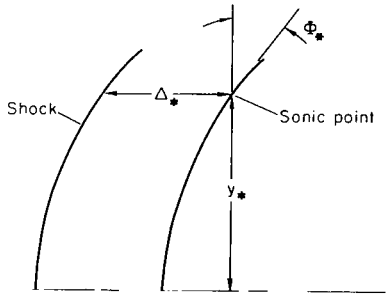

Sketch (a)

B_b (see Notation). Details of the solution are presented in appendix A. The essential result is

$$\frac{[(B_b - 1)\sin^2 \Phi_* + 1]^2}{2(B_b - 1)\sin \Phi_*} \left\{ \frac{1}{\sqrt{B_b - 1}} \sin^{-1} \left[\frac{\sqrt{B_b - 1}\, \sin \Phi_*}{\sqrt{(B_b - 1)\sin^2 \Phi_* + 1}} \right] - \frac{\sin \Phi_*}{(B_b - 1)\sin^2 \Phi_* + 1} \right\}$$

$$= (1 - \sin^2 \Phi_*) - \frac{p_*}{p_{st}} \qquad (2)$$

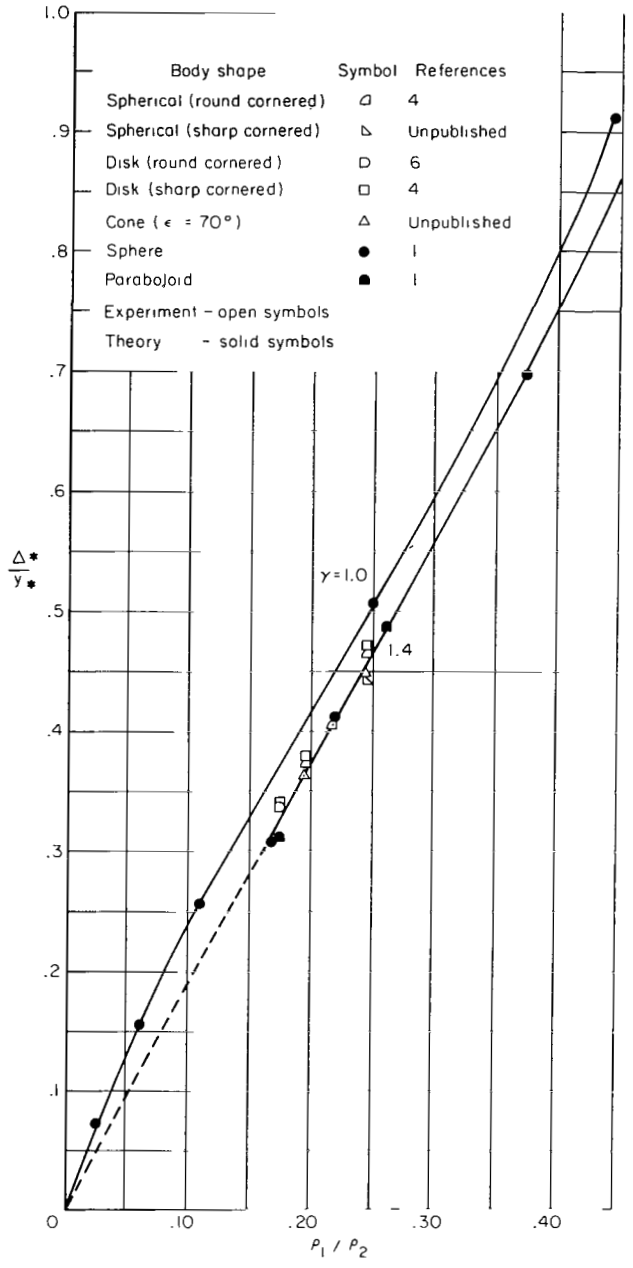

Figure 2.- Correlation curves of shock-standoff distance at sonic point, Δ_*/y_*.

In the present application of equation (2), the gas was assumed perfect. Since the theory requires an infinite shock-density ratio, the value $p_*/p_{st} = 0.607$, appropriate to a gas with $\gamma = 1.0$, was used.

The results of equation (2) for $\sin \Phi_*$ are presented in figure 3 normalized with respect to the value for a sphere ($\sin \Phi_{*1}$). This normalized value is plotted as a function of the more tangible variable, $a/b = B_b^{-1/2}$, rather than as a function of B_b.

Although the absolute value for $\sin \Phi_*$ given by equation (2) may not be correct for a finite density ratio, it is assumed that the ratio $\sin \Phi_*/\sin \Phi_{*1}$ will not differ greatly from that given by exact theory.[1] Thus, if the value of $\sin \Phi_{*1}$ is known for a sphere in a given free stream, the value of $\sin \Phi_*$ for an ellipsoid can be determined from the curve of figure 3. Values of Φ_{*1}, for a sphere at various free-stream conditions (ref. 1) are presented in figure 4 for convenience in such calculations.

If a blunt body does not have a conic section, the parameter B_b is not appropriate. However, the

[1]The validity of figure 3 for finite shock-density ratios is substantiated to some degree by the points from reference 1 for ellipsoids of moderate values of a/b.

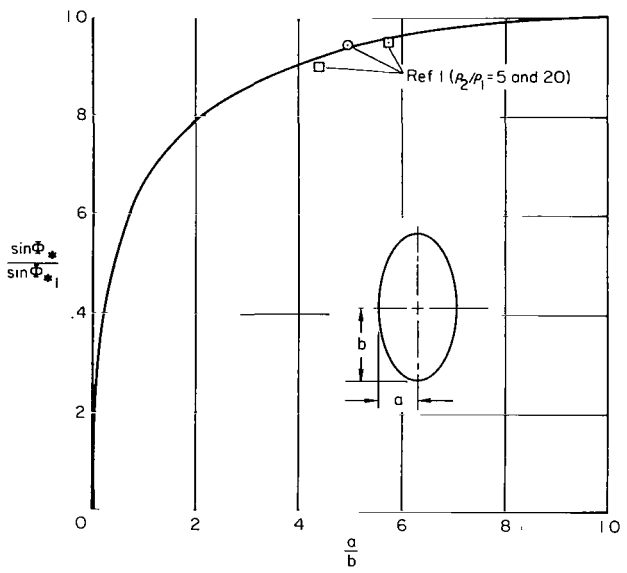

Figure 3.- Sonic angle, Φ_*, on ellipsoids.

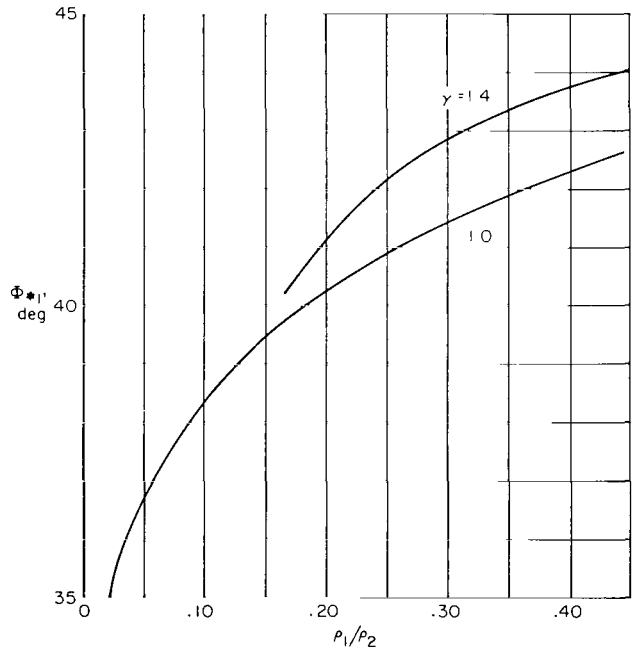

Figure 4.- Sonic angle for a sphere (B_b = 1, a/b = 1).

sonic-point location on other types of blunt bodies may be estimated on the basis of the foregoing analysis. To this end, it is assumed that a shock in the form of a conic section is appropriate to all classes of blunt bodies considered here. For example, a blunt body with a rounded corner of radius r_c is illustrated in sketch (b). When the flow has an infinite shock-density ratio (ρ_2/ρ_1), the shock approaches coincidence with the body in the vicinity of the sonic point. If the sonic point is on the rounded corner of the body, the above Busemann solution applies if the body corner radius r_c is equated to the radius R_{b*} of a conic-section body at the same sonic point ordinate, y_*.

$$\frac{y_*}{R_{b*}} = \sin\Phi_*[(B_b - 1)\sin^2\Phi_* + 1]$$

$$= \frac{y_*}{r_c} = \frac{r_m - r_c(1 - \sin\Phi_*)}{r_c}$$

or

$$\frac{r_c}{r_m} = \frac{1}{1 + (B_b - 1)\sin^3\Phi_*} \qquad (3)$$

Equation (3) gives the r_c/r_m value for an equivalent body that supports the same elliptical shock and the same sonic angle as a body

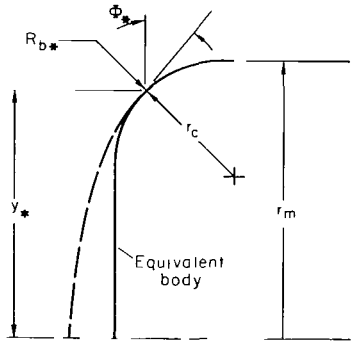

Sketch (b)

with the bluntness parameter, B_b. The relationship between B_b and Φ_* was previously derived and is given by equation (2). The value of $\sin \Phi_*$ normalized with respect to the value for a sphere is plotted in figure 5 as a function of r_c/r_m as determined from equation (3). The general validity of this function at finite shock-density ratios will be discussed in a later section.

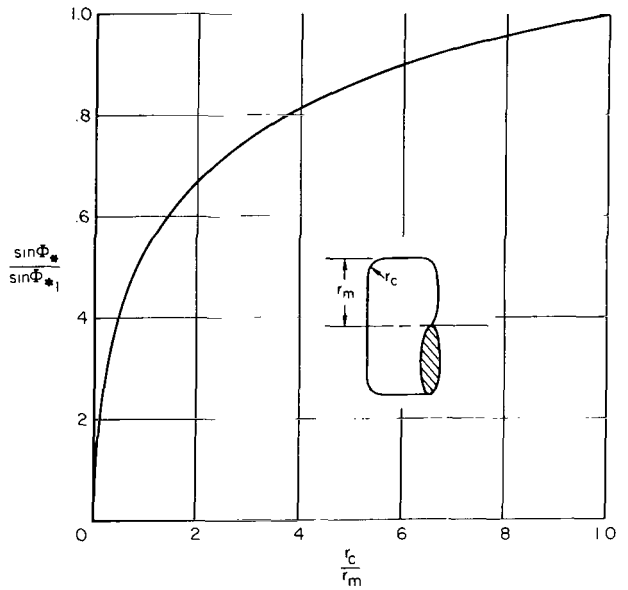

Figure 5.- Sonic angle, Φ_*, on round-cornered bodies.

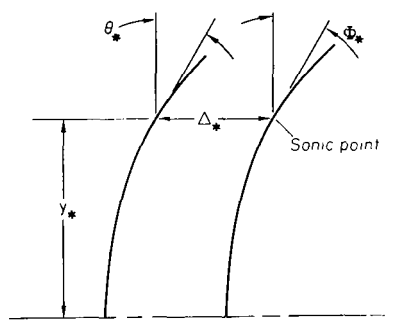

Sketch (c)

Figure 5 is intended to apply to any blunted body with a rounded corner. In many cases, however, a qualification of the sonic angle is necessary, for example when the body is conically or spherically blunted. The conical or spherical portion of the body will be tangent to the corner radius, r_c, at which point a surface inclination angle, ϵ, is defined with respect to a plane normal to the body axis of symmetry. The sonic angle is then taken as ϵ if ϵ is greater than Φ_* determined from figure 5.

Relationship between shock and body inclination.- Reference 2 shows that in a given free stream the shock angle, θ_*, opposite the sonic point on the body is uniquely related to the sonic point angle, Φ_*. The orientation of these angles is shown in sketch (c). The results of reference 2 are restricted to sharp-cornered bodies and are based on a gross mass-flow continuity analysis. It is nevertheless assumed that such a unique angle correspondence does exist and holds for all bodies with a detached shock. If this assumption is valid, the functional relationship between θ_* and Φ_* can be established from any set of shock solutions. The solutions of reference 1 for conic-section bodies were used for this purpose in the following manner: The value of y_*/R_s was found by solving equation (4) (appendix B); values of B_b, B_s, R_s/R_b, and Δ_o/R_s were obtained from reference 1 and the value Δ_*/y_* from figure 2:

$$\frac{\Delta_* y_*}{y_* R_s} = \frac{\Delta_o}{R_s} + \frac{R_b}{B_b R_s}\left[1 - \sqrt{1 - B_b\left(\frac{R_s y_*}{R_b R_s}\right)^2}\right] - \frac{1}{B_s}\left[1 - \sqrt{1 - B_s\left(\frac{y_*}{R_s}\right)^2}\right] \qquad (4)$$

With the value of y_*/R_s determined, the following equations were then solved for θ_* and Φ_*:

$$\tan \theta_* = \frac{\frac{y_*}{R_s}}{\sqrt{1 - B_s \left(\frac{y_*}{R_s}\right)^2}} \tag{5}$$

$$\tan \Phi_* = \frac{\frac{y_* R_s}{R_s R_b}}{\sqrt{1 - B_b \left(\frac{y_* R_s}{R_s R_b}\right)^2}} \tag{6}$$

The above procedure, giving the relationship between θ_* and Φ_*, was restricted to the limited range of body bluntness ($B_b < 3$) (as found in ref. 1) and, therefore, to a limited range of Φ_*. Additional procedures were necessary to determine the value of θ_* at smaller values of Φ_* associated with bodies of larger bluntness. A simple solution for θ_* in the limiting case of a flat disk ($B_b = \infty$, $\Phi_* = 0^\circ$) was found (appendix C). The relationship between θ_* and Φ_* over the range of Φ_* not amenable to available theory was then approximated in the following manner.

It was assumed that if the corner of a flat disk was rounded to a small radius, no important change in the shock shape would occur.[2] For the sonic point on the rounded corner the inclination Φ_* could be significantly different from zero. In the limit of a vanishingly small corner radius, no change occurs in the shock and, therefore, $d\theta_* = 0$. It then follows that $d\theta_*/d\Phi_* = 0$ at $\Phi_* = 0^\circ$, suggesting that θ_* would develop in an even power series in Φ_*. Accordingly, a three-term power series in Φ_* was used to approximate the variation in θ_* from its value at $\Phi_* = 0^\circ$ to the values of θ_* (and $d\theta_*/d\Phi_*$) in the range of Φ_* determined from the results of reference 1.

[2]The small variation in shock shape with changes in body shape is pointed out in reference 1.

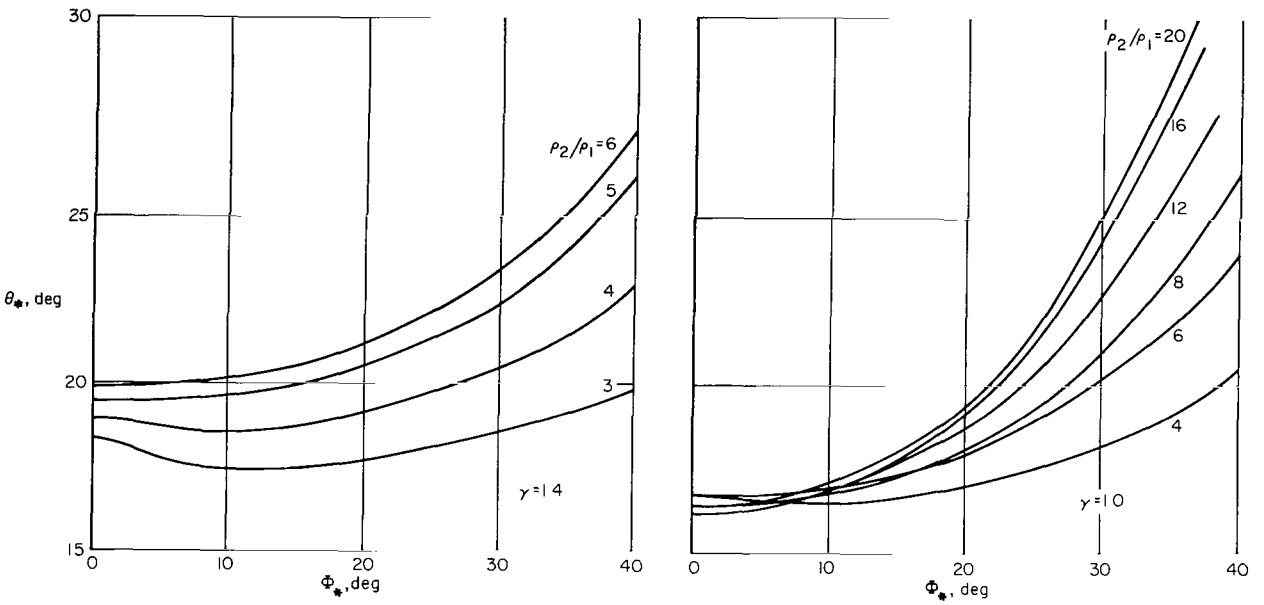

(a) θ_* as a function of Φ_*.

Figure 6.- Inclination angles θ_* and Φ_*.

Plots of θ_* as a function of Φ_* are presented in figure 6(a) for various shock-density ratios and γ values of 1.4 and 1.0. A useful correlation between the results for the values of γ is presented in figure 6(b). The ordinate represents the incremental value or change in θ_* (defined as $\theta_* - \theta_{*O}$) as a function of Φ_*. At a given shock-density ratio, this incremental change in θ_* is independent of γ.

These relationships between θ_* and Φ_* do not completely agree with those of reference 2, primarily because of the restrictions imposed on the shock shape in the earlier work.

The manner in which the $\theta_* - \Phi_*$ functions are applied in determining shock solutions for the classes of bodies considered here will be discussed in the following sections.

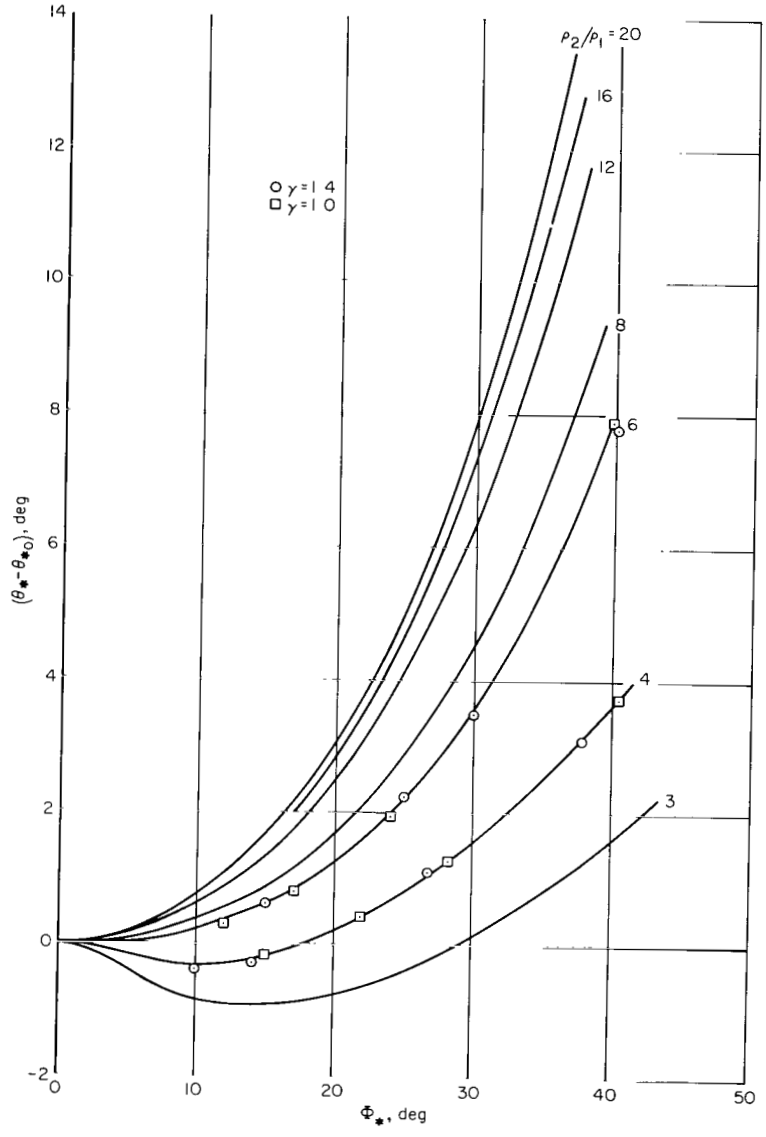

(b) $(\theta_* - \theta_{*O})$ as a function of Φ_*.

Figure 6.- Concluded.

Shock Envelope Solutions

Shock solutions will be considered for the following classes of bodies: ellipsoids ranging from a sphere to a flat disk, spherical or flat-faced bodies with an arbitrary degree of corner rounding, and spherically blunted, large-apex-angle cones. Equations relating the shock shape with the geometry of these bodies will be given. The use of a nomograph which simplifies the solution of these equations will be discussed.

Shock equations for conic-section body.- A conic-section body of known bluntness, B_b, and a shock bluntness, B_s, at a distance, Δ_o, from the body are depicted in sketch (d). The geometrical relationships are:

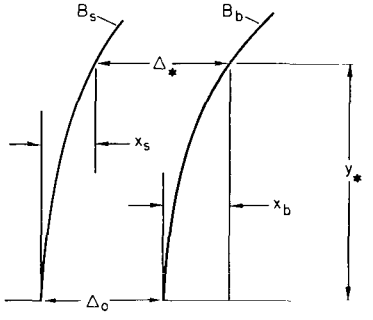

Sketch (d)

$$y_* = \frac{R_b \tan \Phi_*}{\sqrt{1 + B_b \tan^2 \Phi_*}} \tag{7a}$$

$$x_b = \frac{R_b}{B_b}\left(1 - \frac{1}{\sqrt{1 + B_b \tan^2 \Phi_*}}\right) \tag{7b}$$

$$x_s + \Delta_* = \Delta_o + x_b = \Delta_o + \frac{R_b}{B_b}\left(1 - \frac{1}{\sqrt{1 + B_b \tan^2 \Phi_*}}\right) \tag{7c}$$

Equation (7c) is divided by equation (7a) and the result is rearranged to give

$$\frac{\Delta_o}{y_*} = \frac{\Delta_*}{y_*} - \frac{\sqrt{1 + B_b \tan^2 \Phi_*} - 1}{B_b \tan \Phi} + \frac{x_s}{y_*}$$

or

$$\frac{R_s}{y_*} = \left[\frac{\frac{\Delta_*}{y_*} - \frac{\sqrt{1 + B_b \tan^2 \Phi_*} - 1}{B_b \tan \Phi_*}}{\frac{\Delta_o}{R_s}}\right] + \frac{\frac{x_s}{y_*}}{\frac{\Delta_o}{R_s}} \tag{8}$$

Non-conic-section body shock equations.- A section of a body whose geometry[3] involves all the elements of the non-conic-section bodies to be considered is shown in sketch (e). The geometrical relationships are:

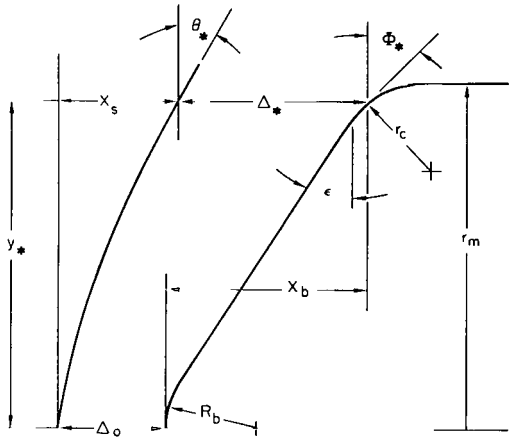

Sketch (e)

$$y_* = r_m - r_c(1 - \sin \Phi_*) \tag{9a}$$

$$x_b = r_m \tan \epsilon + R_b \left(\frac{\cos \epsilon - 1}{\cos \epsilon}\right) + r_c \left(\frac{1 - \sin \epsilon}{\cos \epsilon} - \cos \Phi_*\right) \tag{9b}$$

$$x_s + \Delta_* = \Delta_o + x_b = \Delta_o + r_m \tan \epsilon + R_b \left(\frac{\cos \epsilon - 1}{\cos \epsilon}\right) + r_c \left(\frac{1 - \sin \epsilon}{\cos \epsilon} - \cos \Phi_*\right) \tag{9c}$$

Equation (9c) is divided by equation (9a) and the result is rearranged to give

$$\frac{\Delta_o}{y_*} = \frac{\Delta_*}{y_*} - \frac{r_m \tan \epsilon + R_b \left(\frac{\cos \epsilon - 1}{\cos \epsilon}\right) + r_c \left(\frac{1 - \sin \epsilon}{\cos \epsilon} - \cos \Phi_*\right)}{r_m - r_c(1 - \sin \Phi_*)} + \frac{x_s}{y_*}$$

or

$$\frac{R_s}{y_*} = \left[\frac{\Delta_*}{y_*} - \frac{\tan \epsilon + \frac{R_b}{r_m} \left(\frac{\cos \epsilon - 1}{\cos \epsilon}\right) + \frac{r_c}{r_m} \left(\frac{1 - \sin \epsilon}{\cos \epsilon} - \cos \Phi_*\right)}{1 - \frac{r_c}{r_m}(1 - \sin \Phi_*)} \cdot \frac{\Delta_o}{R_s} \right] + \frac{\frac{x_s}{y_*}}{\frac{\Delta_o}{R_s}} \tag{10}$$

Shock solution nomograph.- The equation of a shock, with the ordinate set equal to y_*, is

$$B_s \frac{x_s}{y_*} = \left(\frac{R_s}{y_*} - \frac{1}{\tan \theta_*}\right) \tag{11}$$

[3]An important additional restriction of the method applies to spherically blunted, large-angle cones: The cone angle $(90^\circ - \epsilon)$ must be sufficiently large to assure a detached shock even if the cone apex is sharp ($R_b = 0$).

Since the body geometry is given, Φ_* can be determined from figure 3 or 5 and the corresponding value for θ_* can then be found from figure 6. Equations (1), (8) (or (10)), and (11) can be solved simultaneously to yield the shock solution in terms of y_*/R_s, B_s, and Δ_o/R_s. This solution requires considerable computation. The computation can be minimized by use of a nomograph consisting of constant B_s and θ_* curves on an R_s/y_* versus x_s/y_* coordinate system. Such curves, calculated with equation (11) and plotted in figure 7, are used as follows.

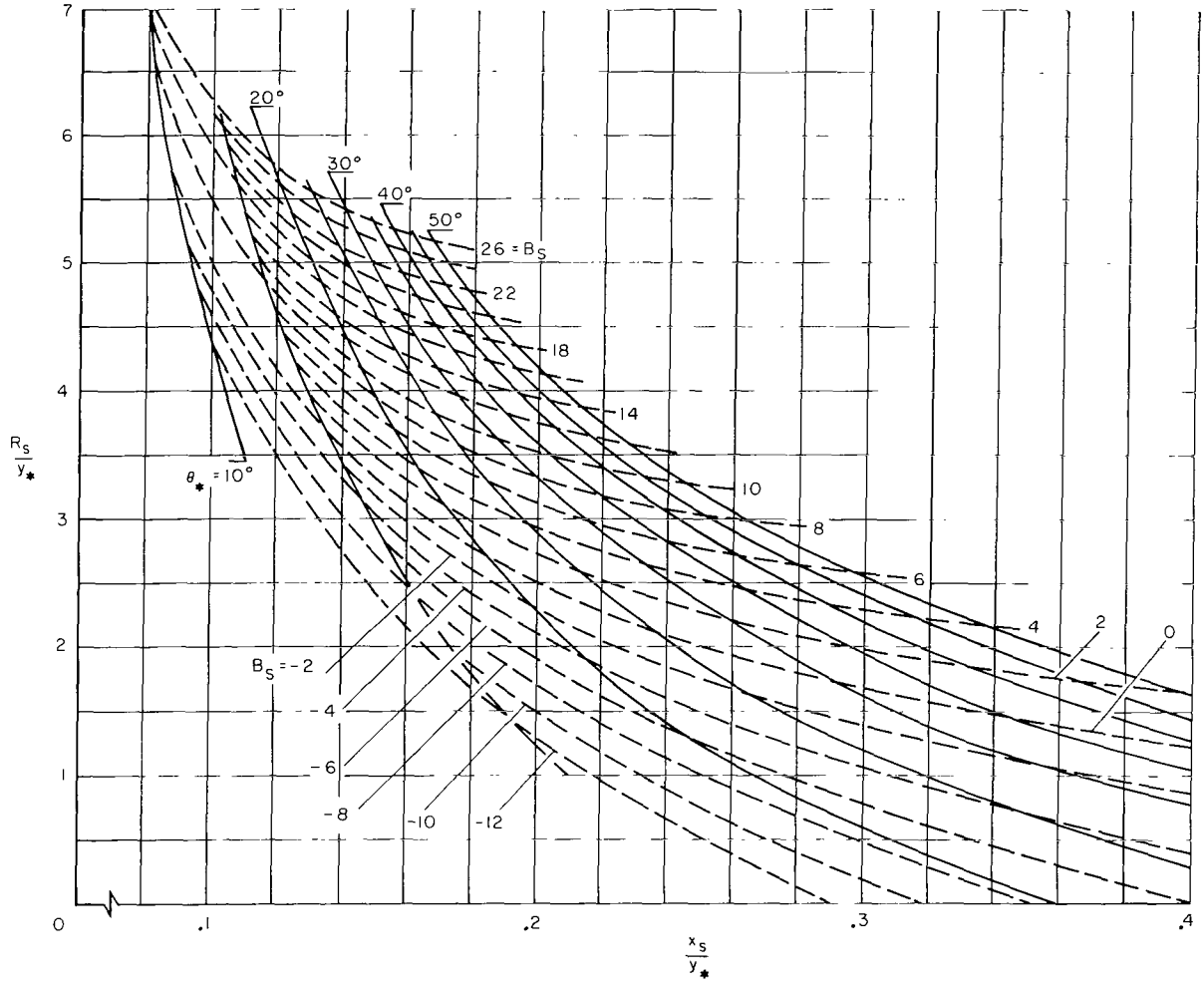

Figure 7.- Shock-solution nomograph.

The numerator of the bracketed term in equation (8) or (10) contains elements of known value. If the value of Δ_o/R_s were also known, equation (8) or (10) could then be plotted as a straight line on the coordinate system. This straight line would have the ordinate value equal to the bracketed term at $x_s/y_* = 0$ and would have a slope equal to R_s/Δ_o. The shock solution would then be given by the intersection of the line with the nomograph curve having the appropriate known value of θ_*. This intersection point simultaneously locates the correct values for B_s and R_s/y_*. The shock shape and its location with respect to the body are then completely defined.

In most cases, Δ_o/R_s is not known so the procedure described above cannot be applied directly. However, a quick convergence to a solution is possible through an iterative technique beginning with a gross initial assumption for the value of Δ_o/R_s. Details of this iterative technique will be clarified in the Numerical Examples section.

Pressure Distribution

The method for estimating the pressure distribution on blunt bodies involves finding the simplest pressure distribution curve that conforms to "end" conditions specified at the stagnation and sonic points on the body. A suitable, easily determined curve was obtained through the use of the following coordinate system.

Coordinate system.- In the natural coordinate system of pressure and location points on the body, pressure can be expressed as some power series in terms of distance from the point of maximum (stagnation) pressure on the body. Experiments indicate that for a flat disk the pressure gradient is infinite at the sonic point (sketch (f)). For such a case, an infinite power series in terms of distance from the sonic point is required to define the pressure distribution. In the present analysis, only a limited number of derivatives could be specified for the pressure distribution so that a term-by-term evaluation of an unlimited power series was not possible. However, if a pressure distribution curve without inflections could be represented in a coordinate system by a curve whose maximum gradient did not exceed a relatively small value, it would then be possible to approximate such a curve with a simple expression of few terms. The coordinate system in sketch (f) was constructed as follows: The origin of the coordinates was at $s/s_* = 0$ and $p/p_{st} = 1$. The axis of the independent variable, s'/s'_*, was directed from this origin to the point $p/p_{st} = p_*/p_{st}$ at $s/s_* = 1$. The transformed coordinates are indicated by dashed lines. The transformed variables are s'/s'_* and z. The absolute value of the slope of the transformed pressure distribution curve, $z = f(s'/s'_*)$, cannot exceed the finite value, $m'_* = 1/m'_{st}$, as indicated. At $s'/s'_* = 0$ and 1, $z = 0$.

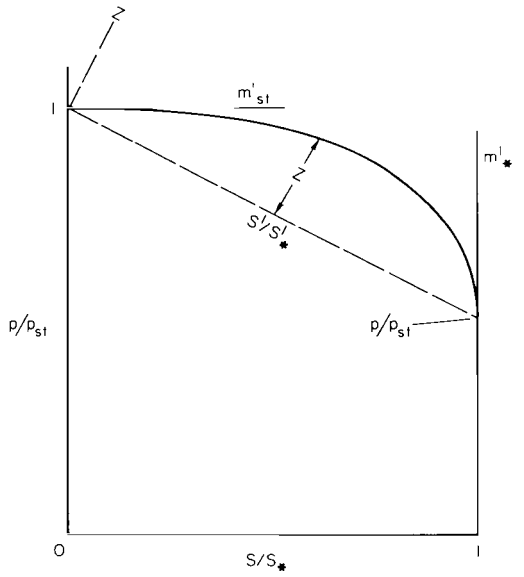

Sketch (f)

The variation of z with s'/s'_* was approximated by two curves having appropriate slopes at $s'/s'_* = 0$ and $s'/s'_* = 1$, respectively, and which were matched to a common tangent. The evaluation of these slopes, the resulting transformed pressure distribution functions, and the method of matching these functions to a common tangent are described in the following paragraphs.

Stagnation point.- The relationship between pressure and velocity for a perfect gas is

$$\frac{p}{p_{st}} = \left[1 - \frac{\gamma - 1}{\gamma + 1}\left(\frac{V}{V_*}\right)^2\right]^{\frac{\gamma}{\gamma-1}}$$

which, for small velocities, V, near the stagnation point, can be written as

$$\frac{p}{p_{st}} \cong 1 - \frac{\gamma}{\gamma + 1}\left(\frac{V}{V_*}\right)^2 \tag{12}$$

The velocity variation with distance, s, is linear near the stagnation point so that equation (12) may be written, in natural coordinates, as

$$\frac{p}{p_{st}} = 1 - \left[\nu \frac{s_*}{\Delta_o}\left(1 + \frac{\Delta_o}{R_b}\right)\right]^2 \left(\frac{s}{s_*}\right)^2 \tag{13}$$

The bracketed term in equation (13) is discussed in detail in appendix D. The transformed function, z, in equation (14) is obtained from the Taylor series expansion in the neighborhood of the stagnation point where the second derivative is obtained from the radius of curvature found from equation (13):

$$z = m'_{st}\left(\frac{s'}{s'_*}\right) - (1 + m'^2_{st})^{3/2}\left[\nu \frac{s_*}{\Delta_o}\left(1 + \frac{\Delta_o}{R_b}\right)\right]^2 \left(\frac{s'}{s'_*}\right)^2 \tag{14}$$

Equation (14) is assumed to give a close approximation to the value of z over a range of s'/s'_* to a matching point value that remains to be determined and depends upon the slope of z at the sonic point.

Sonic point.- Experimental pressure distribution data for flat-faced, round-cornered bodies indicate that the slope of the pressure distribution curve was inversely proportional to the radius of the body at the point where the pressure attained sonic value. The slope or derivative of the pressure distribution curve at the sonic point can be estimated quantitatively on the basis of an approximate theory discussed in appendix D. The result in natural coordinates is

$$\frac{d\left(\frac{p}{p_{st}}\right)}{d\left(\frac{s}{s_*}\right)} \approx - \frac{s_*}{r_c} \tag{15}$$

The slope of z at $s'/s'_* = 1$ (sonic point) is

$$\frac{dz}{d\left(\frac{s'}{s'_*}\right)} = -\tan\left[\cot^{-1} m'_{st} - \cot^{-1}\left(\frac{s_*}{r_c}\right)\right] = -m'_* \tag{16}$$

in transformed coordinates.

Matching of curves.- Equation (14) is assumed to be valid over a range of s'/s'_* from zero to s'_t/s'_*. At s'_t/s'_* the curve defined by equation (14) is tangent to a second curve valid over the range $s'_t/s'_* < s'/s'_* < 1$. The equation of the second curve is assumed to have the same form as equation (14):

$$z = m'_*\left(1 - \frac{s'}{s'_*}\right) - C\left(1 - \frac{s'}{s'_*}\right)^2 \tag{17}$$

The independent variable $1 - (s'/s'_*)$ is used for convenience.

Equations (14) and (17) are equated at s'_t/s'_*. The derivative of equation (14) with respect to s'/s'_* is equated to that of equation (17). Two independent equations are then made available to solve for the constant C in equation (17) and the point of tangency, s'_t/s'_*. The results are

$$\frac{s'_t}{s'_*} = \frac{m'_* - m'_{st}}{m'_* + m'_{st} - 2A} \tag{18a}$$

where A is the absolute value of the coefficient of $(s'/s'_*)^2$ in equation (14) and

$$C = \frac{m'_{st} + m'_* - 2A\,\frac{s'_t}{s'_*}}{2\left(1 - \frac{s'_t}{s'_*}\right)} \tag{18b}$$

The curves given by equations (14) and (17) are plotted over their respective ranges of applicability in the $Z - (s'/s'_*)$ coordinate system. To transform the results into the natural coordinate system, p/p_{st} versus s/s_*, it is only necessary to superpose the natural coordinates onto the $z - (s'/s')$ curves. This is automatically accomplished with double coordinate paper (fig. 10).

The above procedure cannot predict pressure distributions if inflections in pressure occur. Such conditions can occur for a large-angle cone with the apex blunted by a small radius, R_b. However, this case is excluded and the method is applicable whenever $s'_t/s'_* > 0$ (eq. (18a)).

NUMERICAL EXAMPLES

Shock Solutions

The following numerical examples illustrate how the shape of the bow shock and its proximity to the body are determined for typical vehicles from each of the classes considered.

Example A. Ellipsoid: $a/b = 0.25$, $\gamma = 1.4$, $M = 10$

At $M = 10$, the normal shock-density ratio for air is $\rho_2/\rho_1 = 5.71$ or $\rho_1/\rho_2 = 0.175$ thus $G = 0.116$ (fig. 1), $\Delta_*/y_* = 0.325$ (fig. 2), $\sin \Phi_*/\sin \Phi_{*1} = 0.825$ (fig. 3; $a/b = 0.25$), $\Phi_{*1} = 40.4^\circ$ (fig. 4), and $B_b = (b/a)^2 = 16$ (by definition).

The values of Φ_* and θ_* are $\Phi_* = \sin^{-1}(0.825 \sin 40.4^\circ) = 32.3^\circ$ and, $\theta_* = 23.8^\circ$ (fig. 6(a)).

Equation (8) now reduces to

$$\frac{R_s}{y_*} = \left[\frac{0.325 - \frac{\sqrt{1 + 16(0.632)^2} - 1}{16(0.632)}}{\frac{\Delta_o}{R_s}} \right] + \frac{\frac{x_s}{y_*}}{\frac{\Delta_o}{R_s}}$$

$$\frac{R_s}{y_*} = \frac{0.155}{\frac{\Delta_o}{R_s}} + \frac{\frac{x_s}{y_*}}{\frac{\Delta_o}{R_s}}$$

The value of Δ_o/R_s is not known and cannot be determined with equation (1b) since the value of R_s/R_b is not known. If Δ_o/R_s is approximated by $\Delta_o/R_s \approx G = 0.116$, the equation for R_s/y_* becomes

$$\frac{R_s}{y_*} = \frac{0.155}{0.116} + \frac{1}{0.116}\frac{x_s}{y_*} = 1.336 + 8.621\frac{x_s}{y_*}$$

The above equation is now plotted on the coordinates of figure 8(a). The equation is a straight line with the ordinate $R_s/y_* = 1.336$ at $x_s/y_* = 0$ and has a slope of 8.621. This line intersects the curve, $\theta_* = 23.8^\circ$, at $R_s/y_* = 2.98$.

A trial value for R_s/R_b may now be determined from equation 7(a):

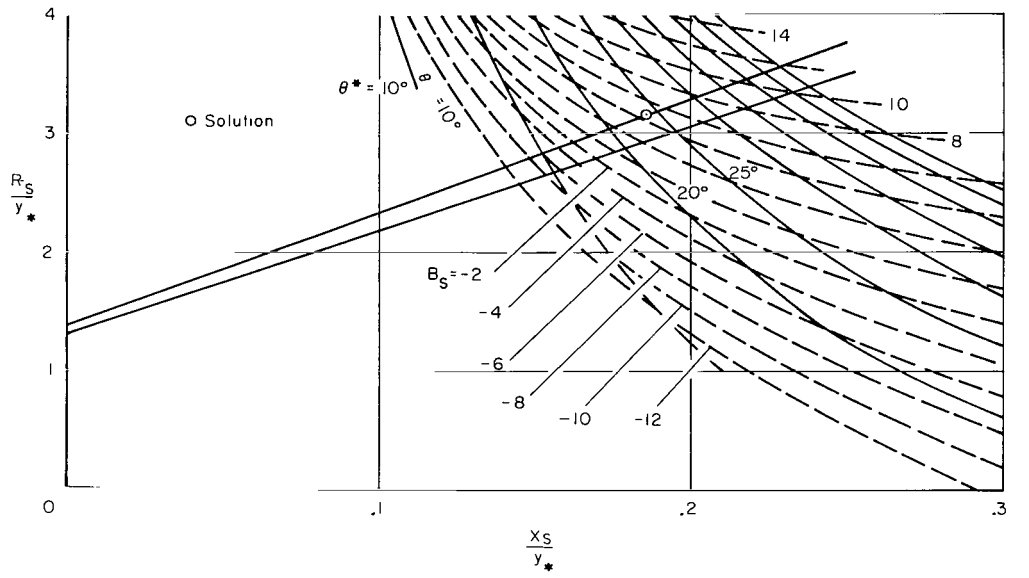

(a) Ellipsoid.

Figure 8.- Numerical application of nomograph.

$$\frac{y_*}{R_b} = \frac{0.632}{\sqrt{1 + 16(0.632)^2}} = 0.232$$

and

$$\frac{R_s}{R_b} = \frac{R_s}{y_*}\frac{y_*}{R_b} = 2.98 \times 0.232 = 0.691$$

The value of Δ_o/R_s, from equation (1b), is

$$\frac{\Delta_o}{R_s} = \frac{\sqrt{1 + 4(0.116)(0.691)} - 1}{2(0.691)} = 0.108$$

which is used to reevaluate R_s/y_*:

$$\frac{R_s}{y_*} = \frac{0.155}{0.108} + \frac{1}{0.108}\frac{x_s}{y_*} = 1.435 + 9.259\frac{x_s}{y_*}$$

and is found to give the value $R_s/y_* = 3.15$ (fig. 8(a)) as the second trial solution. New values of R_s/R_b and Δ_o/R_s are calculated:

$$\frac{R_s}{R_b} = 3.15 \times 0.232 = 0.731$$

and

$$\frac{\Delta_o}{R_s} = \frac{\sqrt{1 + 4(0.116)(0.731)} - 1}{2(0.731)} = 0.108$$

No change in Δ_o/R_s has occurred so convergence to a solution has been achieved. The value for B_s is determined by the intersection point of the final equation for R_s/y_* with the curve, $\theta = 23.8^\circ$ (fig. 8(a)). The final results are:

$$B_s = 4.8$$

$$\frac{\Delta_o}{R_s} = 0.108$$

and

$$\frac{\Delta_o}{R_b} = 0.079$$

Example B. Flat-faced body with rounded corner: $r_c/r_m = 0.25$, $\gamma = 1.4$, $M = 5$

At $M = 5$, the normal shock-density ratio for air is $\rho_2/\rho_1 = 5.00$ or $\rho_1/\rho_2 = 0.200$; thus $G = 0.132$ (fig. 1), $\Delta_*/y_* = 0.372$ (fig. 2), $\sin \Phi_*/\sin \Phi_{*1} = 0.712$ (fig. 5), and $\Phi_{*1} = 41.1^\circ$ (fig. 4). The values $\epsilon = 0^\circ$ and $R_b = \infty$ are appropriate to a flat-faced body.

The values of Φ_* and θ_* are $\Phi_* = \sin^{-1}(0.712 \sin 41.1^\circ) = 27.9^\circ$ and $\theta_* = 21.8^\circ$ (fig. 6(a)).

Equation (10) is now evaluated. (Note that since $R_b = \infty$, equation (1) gives $\Delta_o/R_s = G = 0.132$.)

$$\frac{R_s}{y_*} = \frac{0.372 - \dfrac{0.0 + 0.0 + 0.250(1 - 0.884)}{1 - 0.250(1 - 0.468)}}{0.132} + \frac{\dfrac{x_s}{y_*}}{0.132}$$

$$\frac{R_s}{y_*} = 2.568 + 7.576 \frac{x_s}{y_*}$$

The line represented by the above equation has the R_s/y_* ordinate value of 2.568 at $x_s/y_* = 0$ and a slope of 7.576. This line intersects the curve, $\theta_* = 21.8^\circ$, in figure 8(b) at $R_s/y_* = 3.77$ and also gives $B_s \approx 8.0$. No iteration is necessary since $R_s/R_b = 0$ remains fixed. The shock centerline radius and standoff distance may be related to the body radius, r_m, with equation 9(a):

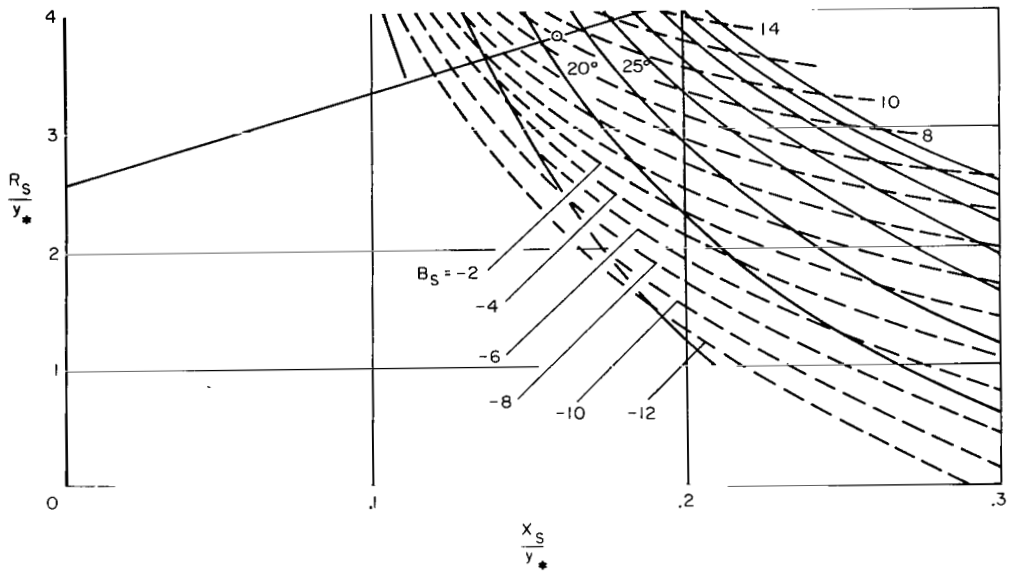

(b) Flat faced body.

Figure 8.- Continued.

$$\frac{y_*}{r_m} = 1 - 0.250(1 - 0.468) = 0.867$$

then

$$\frac{R_s}{r_m} = \frac{R_s}{y_*}\frac{y_*}{r_m} = 3.77 \times 0.867 = 3.27$$

and

$$\frac{\Delta_o}{r_m} = \frac{\Delta_o}{R_s}\frac{R_s}{r_m} = 0.132 \times 3.27 = 0.432$$

The final results are $B_s = 8.0$, $R_s/r_m = 3.27$, and $\Delta_o/r_m = 0.432$.

Example C. Spherically blunted 65° cone with rounded corner: $R_b/r_m = 0.167$, $r_c/r_m = 0.083$, $\gamma = 1.4$, $M = 5.2$

At $M = 5.2$, the normal shock-density ratio of air is $\rho_2/\rho_1 = 5.064$ or $\rho_1/\rho_2 = 0.1975$; thus $G = 0.1305$ (fig. 1), $\Delta_*/y_* = 0.368$ (fig. 2), $\sin \Phi_*/\sin \Phi_{*1} = 0.500$ (fig. 5), and $\Phi_{*1} = 41.05°$ (fig. 4). The value $\epsilon = 90° - 65° = 25°$.

The angle $\Phi_* = \sin^{-1}(0.500 \sin 41.05°) = 19.2°$. However, this value for Φ_* is smaller than $\epsilon = 25°$, the angle of tangency between the corner radius and the conical surface. Therefore, the sonic point is taken at the point of tangency:

$$\Phi_* = \epsilon = 25^\circ$$

and

$$\theta_* = 21.4^\circ \text{ (fig. 6(a))}$$

Equation (10) reduces to

$$\frac{R_s}{y_*} = \frac{0.368 - \dfrac{0.466 + 0.167\left(\dfrac{0.906 - 1}{0.906}\right) + 0.083\left(\dfrac{1 - 0.423}{0.906} - 0.906\right)}{1 - 0.083(1 - 0.423)}}{\dfrac{\Delta_o}{R_s}} + \frac{\dfrac{x_s}{y_*}}{\dfrac{\Delta_o}{R_s}}$$

$$\frac{R_s}{y_*} = \frac{-0.080}{\dfrac{\Delta_o}{R_s}} + \frac{\dfrac{x_s}{y_*}}{\dfrac{\Delta_o}{R_s}}$$

The value of Δ_o/R_s, as in example A, is not known. If Δ_o/R_s is approximated by $G = 0.1305$

$$\frac{R_s}{y_*} = \frac{-0.080}{0.1305} + \frac{1}{0.1305}\frac{x_s}{y_*} = -0.613 + 7.663\frac{x_s}{y_*}$$

In this case, the line representing equation (10) crosses the abscissa axis of figure 8(c) at $x_s/y_* = 0.080$ (independent of the value for Δ_o/R_s)

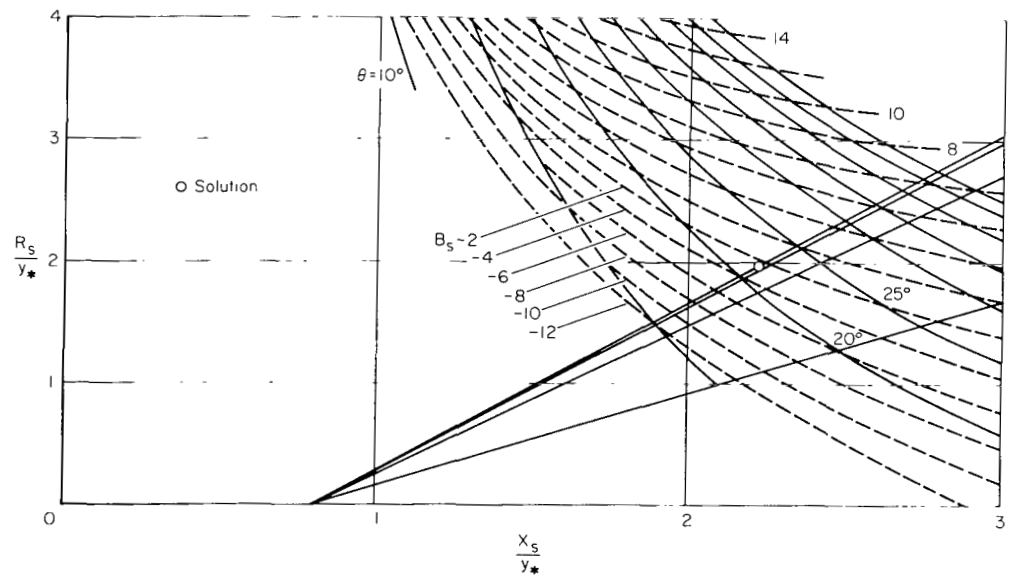

(c) Spherically blunted cone.

Figure 8.- Continued.

and has a slope of 7.663. The intersection of this line with the curve $\theta_* = 21.4^\circ$ gives $R_s/y_* = 1.34$.

A trial value for R_s/R_b may now be determined. Equation (9a) gives

$$\frac{y_*}{r_m} = 1 - 0.083(1 - 0.423) = 0.9519$$

and

$$\frac{R_s}{R_b} = \frac{R_s}{y_*}\frac{y_*}{r_m}\frac{r_m}{R_b} = 1.34\ \frac{0.9519}{0.167} = 1.34 \times 5.710 = 7.651$$

The value of Δ_o/R_s, determined with equation (1b) using the above value for R_s/R_b, is

$$\frac{\Delta_o}{R_s} = \frac{\sqrt{1 + 4(0.1305)(7.651)} - 1}{2(7.651)} = 0.0807$$

Equation (10), reevaluated with the new value for Δ_o/R_s, is

$$\frac{R_s}{y_*} = \frac{-0.080}{0.0807} + \frac{\frac{x_s}{y_*}}{0.0807} = -0.991 + 12.391\ \frac{x_s}{y_*}$$

The intersection of the above line with the curve $\theta_* = 21.4^\circ$ in figure 8(c) gives $R_s/y_* = 1.83$. The adjusted values for R_s/R_b and Δ_o/R_s are

$$\frac{R_s}{R_b} = 1.83 \times 5.710 = 10.449$$

$$\frac{\Delta_o}{R_s} = \frac{\sqrt{1 + 4(0.1305)(10.449)} - 1}{2(10.449)} = 0.0737$$

then

$$\frac{R_s}{y_*} = \frac{-0.080}{0.0737} + \frac{\frac{x_s}{y_*}}{0.0737} = -1.085 + 13.569\ \frac{x_s}{y_*}$$

The intersection of the above adjusted line with the $\theta_* = 21.4^\circ$ curve now gives $R_s/y_* = 1.95$. Another iteration is performed for R_s/R_b and Δ_o/R_s:

$$\frac{R_s}{R_b} = 1.95 \times 5.710 = 11.134$$

and

$$\frac{\Delta_o}{R_s} = \frac{\sqrt{1 + 4(0.1305)(11.134)} - 1}{2(11.134)} = 0.0722$$

Equation (10) is again adjusted to give

$$\frac{R_s}{y_*} = \frac{-0.080}{0.0722} + \frac{\frac{x_s}{y_*}}{0.0722} = -1.108 + 13.850\,\frac{x_s}{y_*}$$

The value $R_s/y_* = 1.97$ is now determined from figure 8(c). No large change in R_s/y_* has occurred, indicating that convergence to a solution has been essentially accomplished. The value $B_s = -2.5$ is also determined from figure 8(c).

The final results are:

$$B_s = -2.5$$

$$\frac{R_s}{R_b} = 1.97 \times 5.710 = 11.249$$

$$\frac{\Delta_o}{R_s} = \frac{1 - 4(0.1305)(11.249)} - 1}{2(11.249)} = 0.0721$$

$$\frac{\Delta_o}{r_m} = \frac{\Delta_o}{R_s}\,\frac{R_s}{y_*}\,\frac{y_*}{r_m} = 0.0721 \times 1.97 \times 0.9519 = 0.135$$

Example D. Spherical-faced body with rounded corner: $R_b/r_m = 2.4$, $r_c/r_m = 0.10$, equilibrium flow with $\rho_2/\rho_1 = 20$

The air is assumed to behave as a perfect gas, and since the Mach number is large, the asymptotic value, $\gamma = [(\rho_2/\rho_1) + 1]/[(\rho_2/\rho_1) - 1] = 21/19 = 1.105$, characterizes the thermodynamic properties of the air.

Since no body shock parameter charts are given here for gases with γ other than 1.0 and 1.4, interpolations are necessary.

The value $G = 0.037$ is found from figure 1 at $\rho_1/\rho_2 = 1/20 = 0.05$. (The effect of γ on G is negligible at small values of ρ_1/ρ_2.) The values $\Delta_*/y_* = 0.117$ is found from figure 2 by linear interpolation between the curves for $\gamma = 1.0$ and $\gamma = 1.4$ at $\rho_1/\rho_2 = 0.05$. The value $\sin \Phi_*/\sin \Phi_{*1} = 0.53$ is found from figure 5 at $r_c/r_m = 0.10$. The value for Φ_{*1} is found from figure 4. Note that there is no great difference between the values of Φ_{*1} for gases with γ of 1.0 or 1.4 at the same shock-density ratio. The difference in Φ_{*1} between gases with $\gamma = 1.1$ and 1.0 should be negligible, particularly at small values of ρ_1/ρ_2. Accordingly, the value $\Phi_{*1} = 36.8^\circ$ found from figure 4 at $\rho_1/\rho_2 = 0.05$ and $\gamma = 1.0$ is assumed valid for $\gamma = 1.105$.

The value of ϵ for a spherically blunted vehicle of radius R_b, tangent to a round corner of radius r_c, is given by

$$\epsilon = \sin^{-1}\left[\frac{\frac{r_m}{R_b}\left(1 - \frac{r_c}{r_m}\right)}{1 - \frac{r_c}{r_m}\frac{r_m}{R_b}}\right] = \sin^{-1}\left[\frac{\frac{1}{2.4}(1 - 0.10)}{1 - \frac{0.10}{2.4}}\right] = 23^\circ$$

The value $\Phi_* = \sin^{-1}(0.53 \sin 36.8^\circ) = 18.4^\circ$. Since the angle ϵ is larger than Φ_*, ϵ is taken as the sonic point inclination angle; therefore, $\epsilon = \Phi_* = 23^\circ$.

The value $\theta_* - \theta_{*o} = 4.2^\circ$ is found from figure 6(b) ($\rho_2/\rho_1 = 20$ and $\Phi_* = 23^\circ$). The curves of figure 6(b) are independent of γ. The value of θ_{*o}, given by equation (C4), is

$$\theta_{*o} = \tan^{-1}\frac{G}{\frac{\Delta_*}{y_*}} = \tan^{-1}\frac{0.037}{0.117} = 17.5^\circ$$

The value of θ_* is found by addition, $(\theta_* - \theta_{*o}) + \theta_{*o} = 17.5^\circ + 4.2^\circ = 21.7^\circ$.

Equation (10) is now evaluated:

$$\frac{R_s}{y_*} = \left[0.117 - \frac{0.424 + 2.4\left(\frac{0.920 - 1}{0.920}\right) + 0.10\left(\frac{1 - 0.391}{0.920} - 0.920\right)}{1 - 0.10(1 - 0.391)}\right] + \frac{\frac{x_s}{y_*}}{\frac{\Delta_o}{R_s}}$$

or

$$\frac{R_s}{y_*} = \frac{-0.084}{\Delta_o/R_s} + \frac{x_s/y_*}{\Delta_o/R_s}$$

If Δ_o/R_s is approximated by $G = 0.037$, the equation for R_s/y_* becomes

$$\frac{R_s}{y_*} = \frac{-0.084}{0.037} + \frac{\frac{x_s}{y_*}}{0.037} = -2.270 + 27.03\frac{x_s}{y_*}$$

In this case, as in example C, the line representing equation (10) crosses the x_s/y_* axis at $x_s/y_* = 0.084$, as is apparent above. The slope of the line is 27.03. The intersection of the line with the $\theta_* = 21.7^\circ$ curve in figure 8(d) gives the value $R_s/y_* = 2.82$.

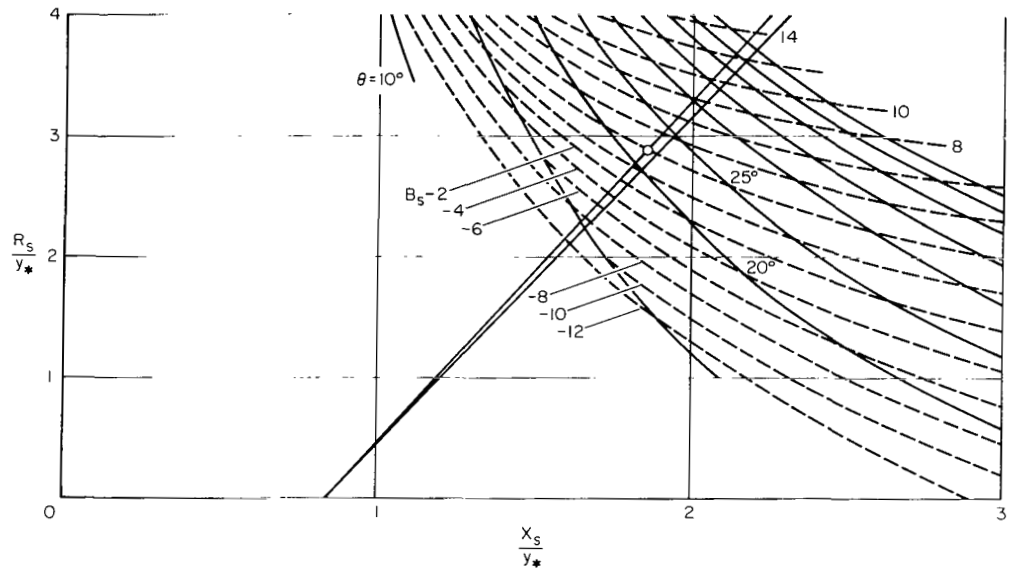

(d) Spherical-faced body.

Figure 8.- Concluded.

Since the sonic point is at the tangent point of R_b and r_c, $y_* = R_b \sin \epsilon$, or $y_*/R_b = \sin 23^\circ = 0.391$. The value for R_s/R_b is then

$$\frac{R_s}{R_b} = \frac{R_s}{y_*}\frac{y_*}{R_b} = 2.82 \times 0.391 \equiv 1.103$$

The value of Δ_o/R_s, determined with equation (1b), is

$$\frac{\Delta_o}{R_s} = \frac{\sqrt{1 + 4(0.037)(1.103)} - 1}{2(1.103)} = 0.0356$$

Equation (10) is reevaluated:

$$\frac{R_s}{y_*} = \frac{-0.084}{0.0356} + \frac{\frac{x_s}{y_*}}{0.0356} = -2.359 + 28.09\,\frac{x_s}{y_*}$$

A new value of $R_s/y_* = 2.93$ is found from figure 8(d). Since the value of R_s/y_* has not changed greatly, convergence to a solution has been essentially achieved. The final values are

$$B_s \approx 2$$

$$\frac{R_s}{R_b} = 2.93 \times 0.391 = 1.146$$

$$\frac{\Delta_o}{R_s} = 0.0356$$

and

$$\frac{\Delta_o}{r_m} = \frac{\Delta_o}{R_s}\frac{R_s}{y_*}\frac{y_*}{r_m} = 0.0356 \times 2.93 \times 0.9391 = 0.098$$

Pressure Distribution

An example calculation for the pressure distribution over the forward face of a blunt body is presented in the following paragraphs. Only one example is given since the calculative procedure, with obvious minor variations, is applicable to most bodies for which the shock solution has been determined.

The method is not applicable to certain cases of large-angle cones with the apex blunted by a small radius, R_b. Criteria for applicability of the method are given in the Analysis section.

The example calculation applies to the round-cornered, flat-faced body at Mach number 5 for which the shock solution was calculated in figure 8(b). The pertinent shock and body parameters are $r_c/r_m = 0.25$, $\Phi_* = 27.9^o$, $\Delta_o/r_m = 0.432$, $\rho_1/\rho_2 = 0.20$, and $\gamma = 1.4$.

First, the numerical values for the coefficients of s'/s'_* and $(s'/s'_*)^2$ of equation (14) are determined. The values for m'_{st}, s_*/Δ_o, Δ_o/R_b, and ν are required. The quantity m'_{st} represents the slope of the line drawn from $p/p_{st} = 1$ to p_*/p_{st} as indicated in sketch (f). In the present example, the gas is air for which $p/p_{st} = 0.528$; and

$$m'_{st} = 1 - \frac{p}{p_{st}} = 1 - 0.528 = 0.472$$

The length, s_*, extends from the stagnation point at the vehicle centerline to the sonic point at location Φ_* on the rounded corner of radius r_c. For the present example, s_* has the value

$$s_* = (r_m - r_c) + \left(\frac{\Phi_* r_c}{57.3^o}\right)$$

which, expressed in terms of Δ_o, is

$$\frac{s_*}{\Delta_o} = \frac{r_m}{\Delta_o}\left(1 - \frac{r_c}{r_m}\right) + \frac{\Phi_*}{57.3}\frac{r_c}{r_m}\frac{r_m}{\Delta_o}$$

or

$$\frac{s_*}{\Delta_o} = \frac{1}{0.432}(1 - 0.25) + \frac{27.9^o}{57.3^o} 0.25 \frac{1}{0.432} = 2.018$$

The value for Δ_o/R_b is 0 since $R_b = \infty$ for a flat face. The value $\nu = 0.150$ is found from figure 9 at $\rho_1/\rho_2 = 0.20$ and $\gamma = 1.4$.

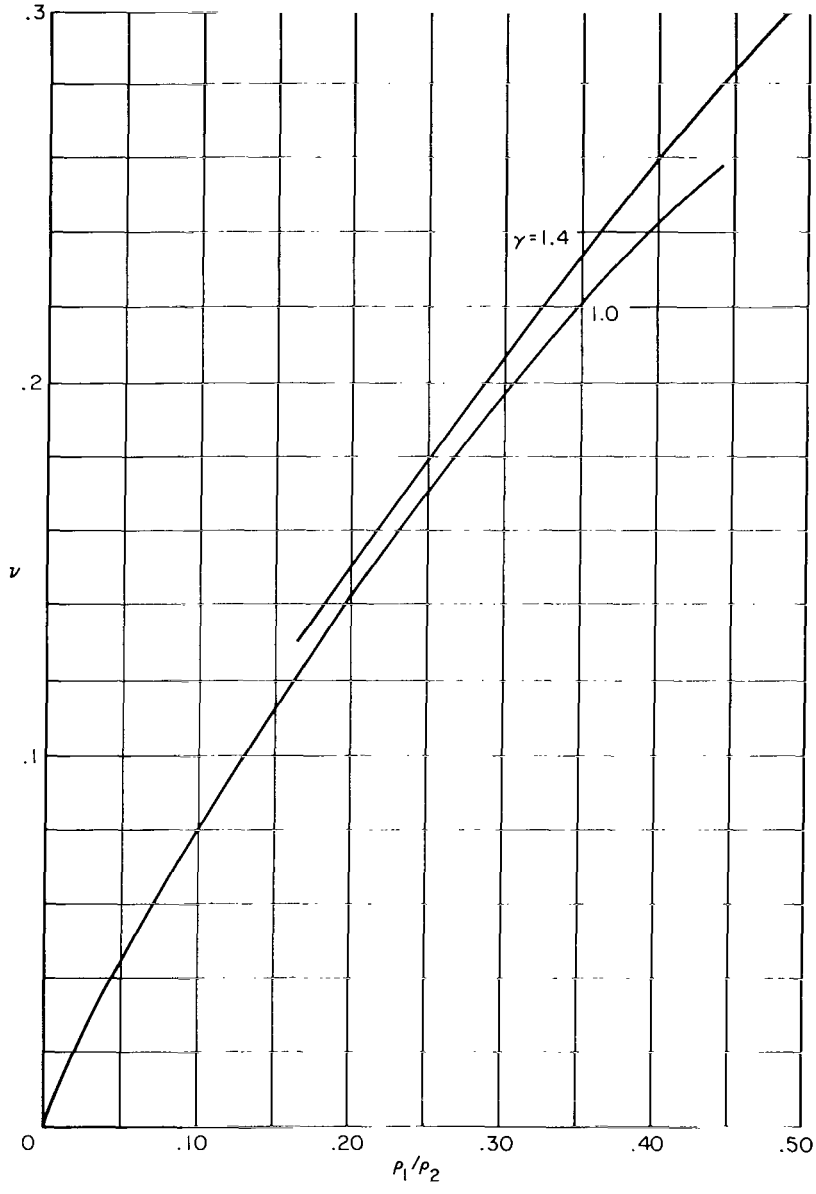

Figure 9.- The ν function.

Equation (14), written with numerical coefficients, is

$$z = 0.472 \frac{s'}{s'_*} - (1 + 0.472^2)^{3/2}[0.150 \times 2.018(1 + 0.0)]^2 \left(\frac{s'}{s'_*}\right)^2$$

or

$$z = 0.472 \frac{s'}{s'_*} - 0.126 \left(\frac{s'}{s'_*}\right)^2$$

Next, the numerical values of the coefficients of $1 - s'/s'_*$ and $[1 - (s'/s'_*)]^2$ of equation (17) are determined. The values for s_*/r_c, m'_*, s'_t/s'_*, and C are required.

$$\frac{s_*}{r_c} = \frac{r_m}{r_c} \frac{\Delta_o}{r_m} \frac{s_*}{\Delta_o} = \frac{1}{0.25} 0.432 \times 2.018 = 3.487$$

Equation (16) is then evaluated for m'_*

$$m'_* = \tan\left(\cot^{-1} m'_{st} - \cot^{-1} \frac{s_*}{r_c}\right) = \tan(\cot^{-1} 0.472 - \cot^{-1} 3.487)$$

$$= \tan (64.7^\circ - 16.0^\circ) = 1.144$$

The value of A required to calculate the value of the coefficient C has already been determined and is the coefficient of $(s'/s'_*)^2$ in the equation for z, that is, A = 0.126. The value of the tangent point location s'_t/s'_* is also required to evaluate C. Its value (given by eq. (18a)) is

$$\frac{s'_t}{s'_*} = \frac{1.144 - 0.472}{1.144 + 0.472 - 2 \times 0.126} = 0.4927$$

The coefficient C (given by eq. (18b)) may now be evaluated:

$$C = \frac{0.472 + 1.144 - 2 \times 0.126 \times 0.4927}{2(1 - 0.4927)} = 1.471$$

Equation (17), written with numerical coefficients, is

$$z = 1.144 \left(1 - \frac{s'}{s'_*}\right) - 1.471 \left(1 - \frac{s'}{s'_*}\right)^2$$

Values for z in the range $0 < s'/s'_* < 0.4927$ computed with equation (14) are

s'/s'_*	z
0.0	0.0
0.1	0.0459
0.2	0.0894
0.3	0.1303
0.4	0.1686
0.4927	0.2019

Values for z in the range $0.4927 < s'/s'_* < 1.0$ computed with equation (17) are

s'/s'_*	z
0.4927	0.2019
0.6	0.2222
0.7	0.2108
0.8	0.1697
0.9	0.0996
1.0	0.0

The above sets of values are shown plotted on the Z - (s'/s'_*) coordinates of figure 10. The resulting curve represents the pressure distribution on the superposed (p/p_{st}) - (s/s_*) coordinates.

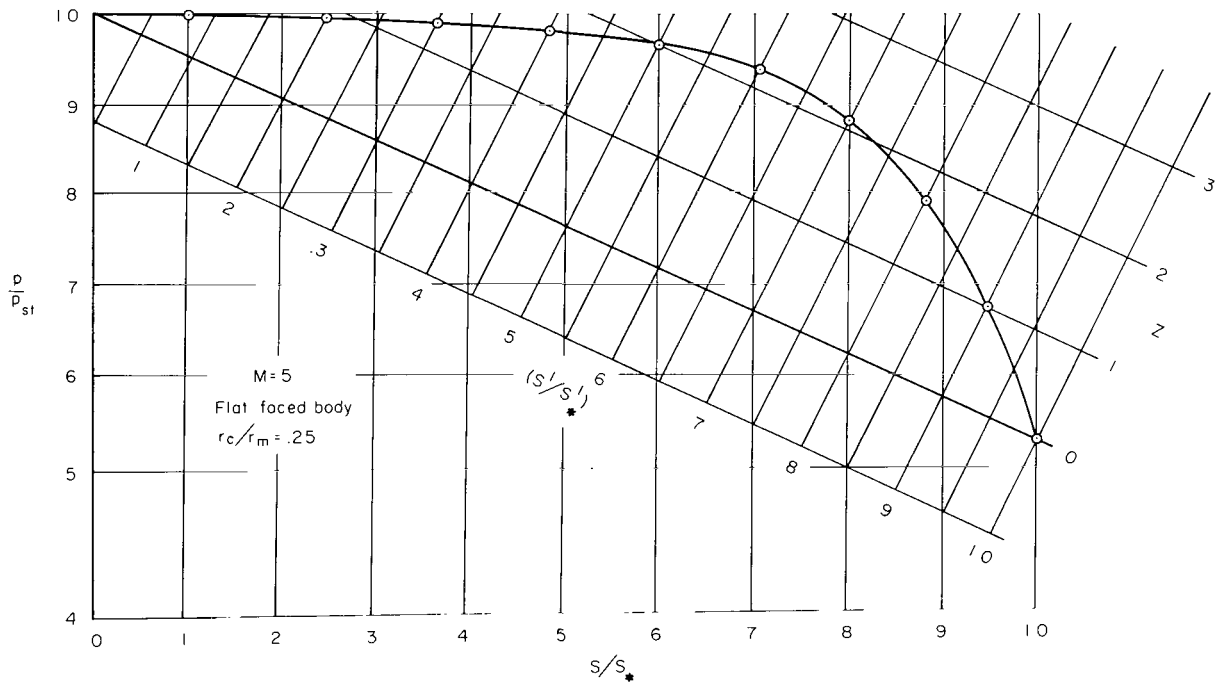

Figure 10.- The Z - (s'/s'_*) coordinate system with an example pressure-distribution solution.

COMPARISON OF EXPERIMENTAL AND PREDICTED RESULTS

The validity of the method was assessed on the basis of the experimental results of references 3, 4, 6, 7, and 8. These data are not extensive but do include representative cases among the classes of body shapes considered in the previous sections.

Shock Shape

A comparison of predicted and experimental shock traces for various types of blunt bodies is shown in figure 11.

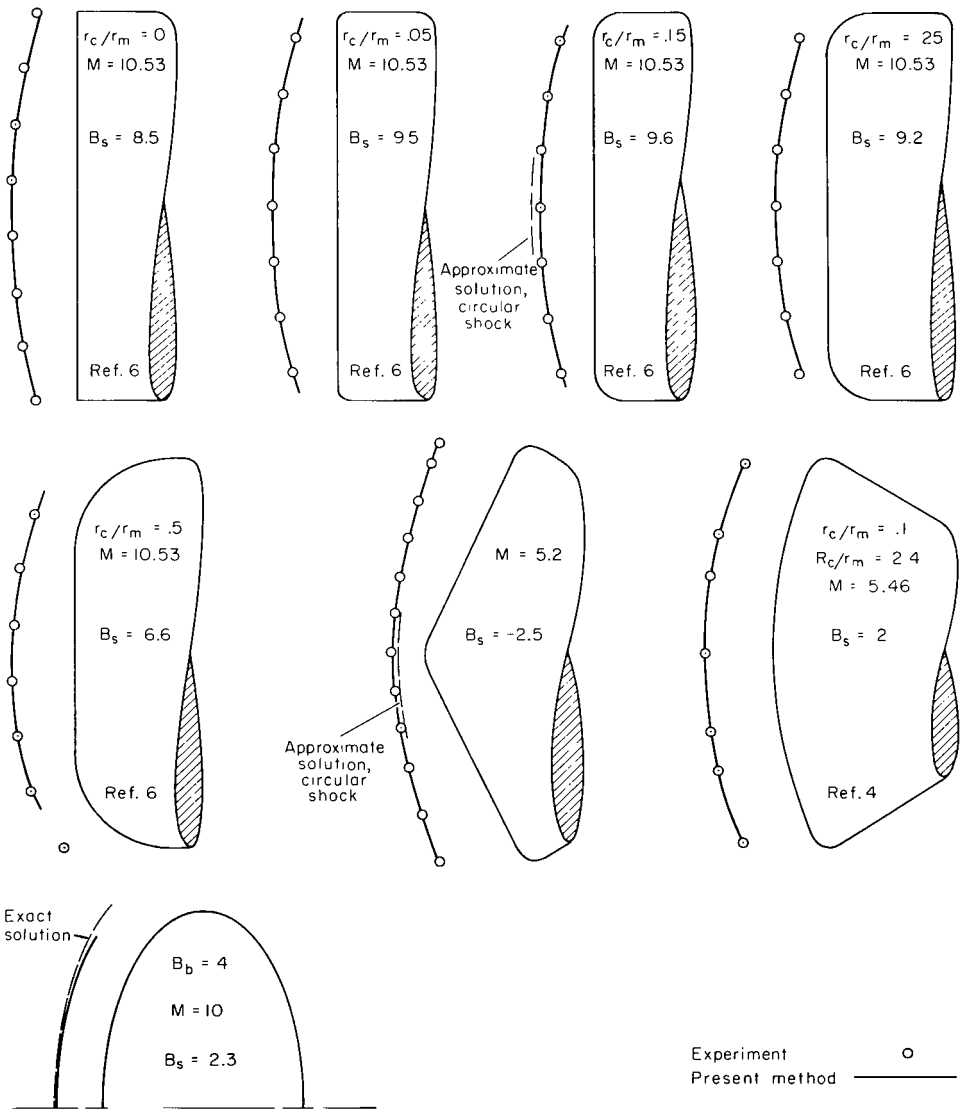

Figure 11.- Comparison of experimental and predicted shock shapes.

The geometric parameters of each body are indicated along with the bluntness, B_S, of the associated shock and the Mach number of the free stream. Good agreement between experimental and predicted shock shapes is shown.

In all cases, the shock traces appear circular. However, the shock bluntness, B_S, has a significant effect on the centerline shock standoff distance. To illustrate this effect, an element of a circular shock is shown on the body axis of symmetry for the cases, $r_c/r_m = 0.5$ and $M = 10.53$, and for the conical body (example C), $M = 5.2$. The circular shock satisfies the value, Δ_*/y_*, appropriate to the free-stream flow and the value, Φ_*, appropriate to the body geometry. An appreciable error is evident in the shock standoff distance at the centerline for the circular shock. This error would increase at larger values for the normal shock-density ratio.

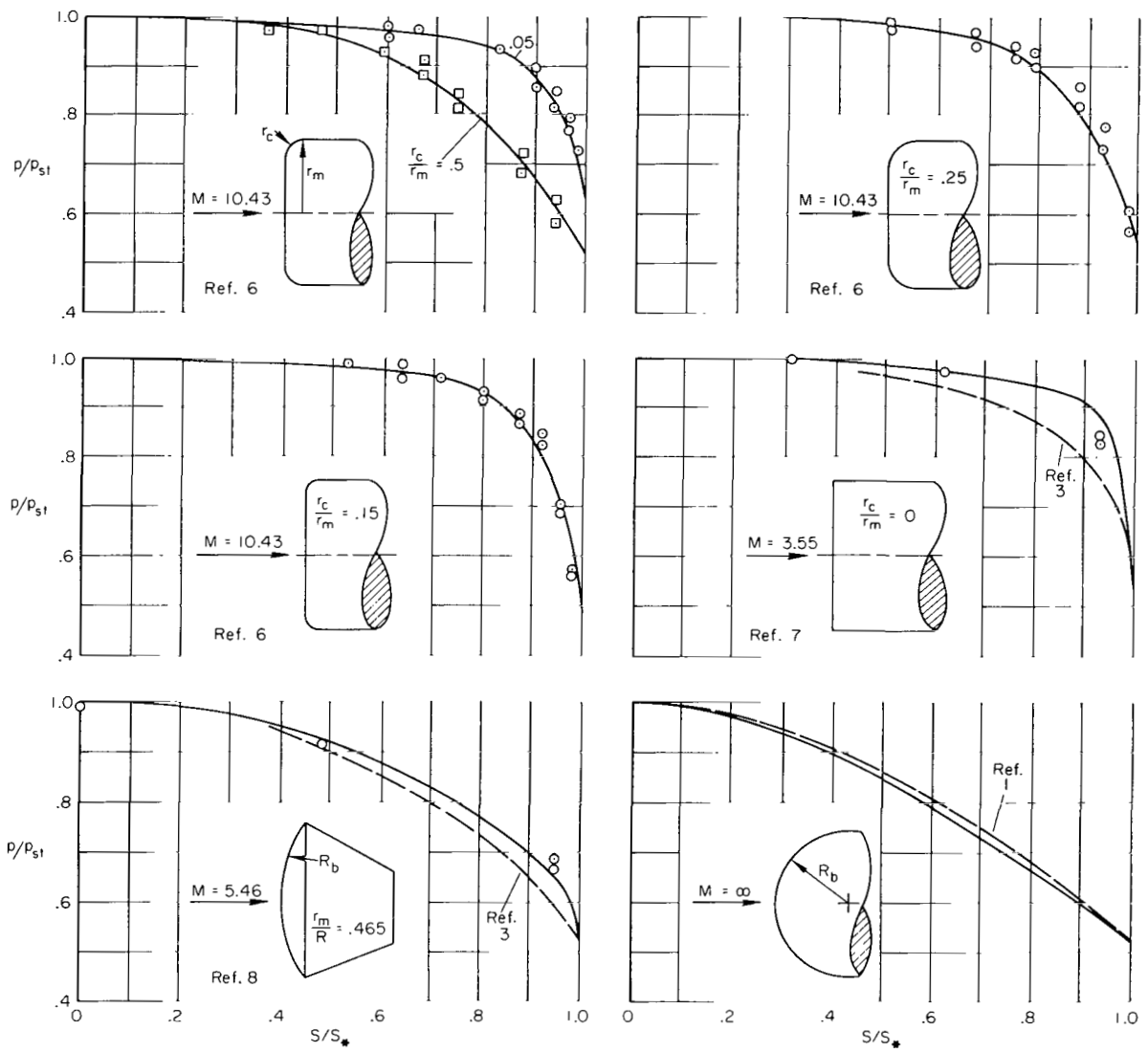

Figure 12.- Comparison of experimental and predicted pressure distributions.

The good agreement between predicted and experimental shock shapes verifies the correlation curve of Δ_*/y_* (fig. 2) and the value, Φ_*, determined from figure 5. The good agreement also confirms the relationship between θ_* and Φ_* (fig. 6) since the value of B_s, which strongly influences the centerline shock standoff distance, is sensitive to the correct value for θ_*.

Pressure Distribution

Predicted and experimental pressure distributions over the forward face of various blunt bodies are compared in figure 12. The results of the present method and the theoretical results of reference 1 for the sphere at $M = \infty$ are also compared.

Agreement between the predicted and experimental results is usually within the scatter of the experimental values. The predicted values are somewhat higher than the experimental values for the sharp-cornered, flat-faced cylinder at $M = 3.55$. Values predicted by the method of reference 3, which is applicable for the two sharp-cornered vehicles shown, are also indicated in figure 12; those predicted by the present method are in better accord with experiment.

CONCLUDING REMARKS

A method was developed for predicting shock envelopes and pressure distributions for a variety of blunt bodies at zero angle of attack. The method is restricted to those cases in which the bow shock is detached from the body and the flow over the forward face of the body is subsonic.

The method is based on correlation functions which relate the shock standoff distances at the stagnation and sonic points to the body geometry. These correlation functions were developed from the perfect gas solutions of reference 1 and depend primarily on the normal-shock density ratio modified to a small degree by the specific heat ratio of the gas. Since the effect of the specific-heat ratio is small, the present method should give adequate solutions for the equilibrium flows of real gases.

Predicted shock envelopes and pressure distributions were compared with experimental values for air flows in the Mach number range of 3.55 to 10.53 for a variety of body shapes. Satisfactory agreement between predicted and experimental values was found for both shock shapes and pressure distributions.

Ames Research Center
National Aeronautics and Space Administration
Moffett Field, Calif., 94035, Nov. 13, 1967
129-01-08-01-00-21

APPENDIX A

SONIC LOCATION ON ELLIPSOIDS

The sonic location on ellipsoids is found by the Busemann solution for infinite shock-density ratio.

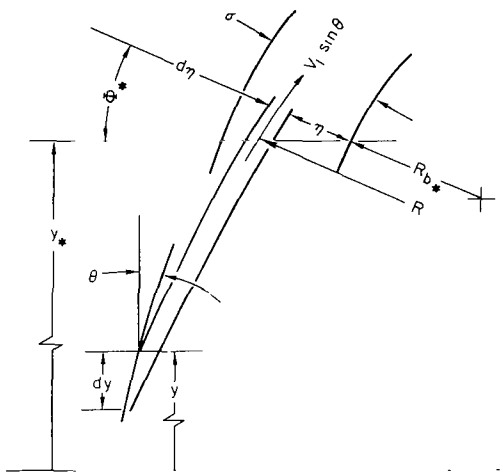

Sketch (g)

The shock-body geometry in the vicinity of the sonic point of an ellipsoid is shown in sketch (g). The shock-layer thickness, σ, is measured normal to the body or in the direction inclined at the angle, Φ_*, with respect to the free-stream direction. The curve of radius, $\mathcal{R}$, represents the streamline passing through the shock at a distance y from the axis of symmetry, at which point the shock inclination is θ. The Busemann assumptions are made that the momentum tangent to the shock is preserved along streamlines within the shock layer, and that the velocity also remains constant along a streamline as indicated. In the limit of a vanishingly thin shock layer, the velocity is $V_1 \sin\theta = V_1 \sin\Phi$ and the stream radius, $\mathcal{R}$, becomes equal to the local body radius, R_{b*}, at the sonic point.

A mass-flow continuity equation involving the differential annular flow tubes at the shock and within the shock layer, relating $d\eta$ and y, is written

$$2\pi\rho_1 V_1 y\, dy = 2\pi\rho_2 V_1 y_* \sin\Phi\, d\eta$$

or

$$\frac{\rho_1 y\, dy}{\rho_2 y_* \sin\Phi} = d\eta \tag{A1}$$

The values of y and Φ for an ellipsoid are related by

$$\frac{y}{R_b} = \frac{\sin\Phi}{\sqrt{(B_b - 1)\sin^2\Phi + 1}} \tag{A2}$$

Equation (A2) is differentiated with respect to Φ with the result

$$\frac{dy}{R_b} = \frac{\cos\Phi\, d\Phi}{[(B_b - 1)\sin^2\Phi + 1]^{3/2}} \tag{A3}$$

The variable y is eliminated from equation (A1) with equations (A2) and (A3):

$$\frac{\rho_1 R_b^2}{\rho_2 y_*} \frac{\cos \Phi \, d\Phi}{[(B_b - 1)\sin^2 \Phi + 1]^2} = d\eta \tag{A4}$$

The differential pressure, Δp, across the shock layer at the sonic point ($\Phi = \Phi_*$) is given by

$$\Delta p = \int_o^\sigma \frac{dp}{d\eta} d\eta = \int_o^\sigma \frac{\rho_2 V_1^2 \sin^2 \Phi \, d\eta}{R_{b*}} = \frac{\rho_1 V_1^2 R_b^2}{y_* R_{b*}} \int_o^{\Phi_*} \frac{\sin^2 \Phi \cos \Phi \, d\Phi}{[(B_b - 1)\sin^2 \Phi + 1]^2}$$

The radius, R_{b*}, of an ellipse at location Φ_* is related to the centerline radius, R_b, by the identity

$$\frac{R_b^2}{y_* R_{b*}} = \frac{[(B_b - 1)\sin^2 \Phi_* + 1]^2}{\sin \Phi_*} \tag{A5}$$

The above integration was performed and, with equation (A5), the result was arranged to give the following equation for the differential pressure across the shock layer at the sonic point:

$$\frac{\Delta p}{\rho_1 V_1^2} = \frac{[(B_b - 1)\sin^2 \Phi_* + 1]^2}{2(B_b - 1)\sin \Phi_*} \left\{ \frac{1}{\sqrt{B_b - 1}} \sin^{-1} \left[\frac{\sqrt{B_b - 1} \sin \Phi_*}{\sqrt{(B_b - 1)\sin^2 \Phi_* + 1}} \right] - \frac{\sin \Phi_*}{(B_b - 1)\sin^2 \Phi_* + 1} \right\} \tag{A6}$$

An independent equation giving this pressure differential for a gas with $\gamma = 1$ at infinite Mach number is the Newtonian result

$$\frac{\Delta p}{\rho_1 V_1^2} = (1 - \sin^2 \Phi_*) - \frac{p_*}{p_{st}} \tag{A7}$$

Equations (A6) and (A7) are equated to give

$$\frac{[(B_b - 1)\sin^2 \Phi_* + 1]^2}{2(B_b - 1)\sin \Phi_*} \left\{ \frac{1}{\sqrt{B_b - 1}} \sin^{-1} \left[\frac{\sqrt{B_b - 1} \sin \Phi_*}{\sqrt{(B_b - 1)\sin^2 \Phi_* + 1}} \right] - \frac{\sin \Phi_*}{(B_b - 1)\sin^2 \Phi_* + 1} \right\}$$

$$= (1 - \sin^2 \Phi_*) - \frac{p_*}{p_{st}} \tag{2}$$

APPENDIX B

THE $\theta_* - \Phi_*$ FUNCTION

The relationship between θ_* and Φ_* was derived from the results from reference 1 for a sphere, along with the results found from the shock solutions of a series of increasingly (elliptically) blunted bodies. The solution for elliptically blunted bodies is developed in this section.

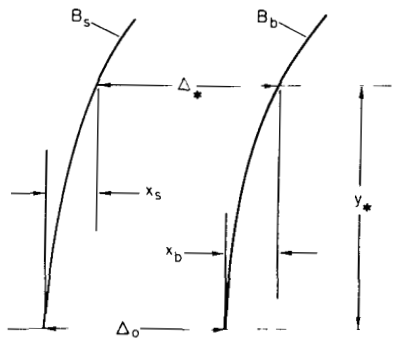

Sketch (h)

Sketch (h) depicts a body that is elliptically blunted, B_b, up to at least the sonic point at y_* and its associated shock of bluntness B_s.

By inspection,

$$\Delta_* = \Delta_o + x_b - x_s \tag{B1}$$

The values of x_s and x_b are related to y through the bluntness parameters, B_s and B_b, as follows:

$$x_s = \frac{R_s}{B_s}\left[1 - \sqrt{1 - B_s\left(\frac{y_*}{R_s}\right)^2}\right] \tag{B2}$$

and

$$x_b = \frac{R_b}{B_b}\left[1 - \sqrt{1 - B_b\left(\frac{y_*}{R_b}\right)^2}\right] \tag{B3}$$

The values of x_s and x_b given by equations (B2) and (B3) are substituted into equation (B1) and the result divided by R_s to give

$$\frac{\Delta_*}{y_*}\frac{y_*}{R_s} = \frac{\Delta_o}{R_s} + \frac{R_b}{B_b R_s}\left[1 - \sqrt{1 - B_b\left(\frac{R_s}{R_b}\frac{y_*}{R_s}\right)^2}\right] - \frac{1}{B_s}\left[1 - \sqrt{1 - B_s\left(\frac{y_*}{R_s}\right)^2}\right] \tag{4}$$

Equation (4) is then solved for y_*/R_s. The angles θ_* and Φ_* are then found from the following equations, which are derivatives of equations (B2) and (B3),

$$\tan\theta_* = \frac{\frac{y_*}{R_s}}{\sqrt{1 - B_s\left(\frac{y_*}{R_s}\right)^2}} \tag{5}$$

$$\tan \Phi_* = \frac{\frac{y_*}{R_s}\frac{R_s}{R_b}}{\sqrt{1 - B_b\left(\frac{y_*}{R_s}\frac{R_s}{R_b}\right)^2}} \qquad (6)$$

APPENDIX C

SHOCK BLUNTNESS B_s AND ANGLE θ_{*o} FOR A DISK

On a flat disk the centerline body radius $R_b = \infty$ and equation (1) gives

$$\frac{\Delta_o}{R_s} = G \tag{C1}$$

The equation of the shock is written in the form

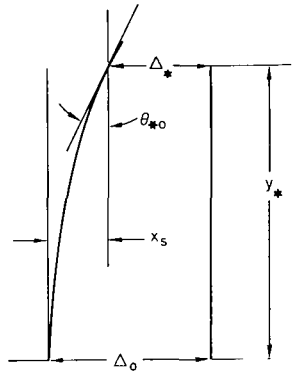

Sketch (i)

$$B_s \frac{x_s}{y_*} = \left(\frac{R_s}{y_*} - \frac{1}{\tan \theta_{*o}}\right) \tag{C2a}$$

where x_s is the streamwise distance from the shock apex to the location on the shock at the distance Δ_* in the free-stream direction from the corner of the disk, as indicated in sketch (i). The angle θ_{*o} is the shock inclination; the length x_s has the value $\Delta_o - \Delta_*$. Substituting this value for x_s in equation (C2a) and with $R_s = \Delta_o/G$ gives

$$B_s \left(\frac{\Delta_o - \Delta_*}{y_*}\right) = \left(\frac{\Delta_o}{y_*}\frac{1}{G} - \frac{1}{\tan \theta_{*o}}\right) \tag{C2b}$$

which is written in the form

$$\frac{\Delta_o}{y_*}\left(\frac{1}{G} - B_s\right) = \frac{\Delta_*}{y_*}\left(\frac{y_*}{\Delta_*}\frac{1}{\tan \theta_{*o}} - B_s\right) \tag{C2c}$$

A solution to equation (C2c) is given if

$$B_s = \frac{1}{G} \tag{C3}$$

and

$$\tan \theta_{*o} = \frac{G}{\frac{\Delta_o}{y_*}} \tag{C4}$$

APPENDIX D

PRESSURE DISTRIBUTION

The pressure distribution at the stagnation and sonic point locations of a body are developed as follows.

Stagnation Point

In reference 2 it is shown that the stagnation point velocity gradient is

$$\frac{dV}{ds} = \frac{V_1}{\Delta_o}\left(1 + \frac{\Delta_o}{R_b}\right)\frac{f}{2} \tag{D1a}$$

The function, f, of reference 2 is related to the function G as follows:

$$f = 2\,\frac{\rho_1}{\rho_{st}}\left[1 - \left(\frac{\rho_2}{\rho_1} - 1\right)G\right] \tag{D1b}$$

Thus,

$$\frac{dV}{ds} = \frac{V_1}{\Delta_o}\left(1 + \frac{\Delta_o}{R_b}\right)\frac{\rho_1}{\rho_{st}}\left[1 - \left(\frac{\rho_2}{\rho_1} - 1\right)G\right] \tag{D1c}$$

If the velocity, V, is assumed to be linear with s in the vicinity of the stagnation point, equation (D1c) may be integrated and normalized with respect to sonic $(\ )_*$ values to yield

$$\frac{V}{V_*} = \frac{V_1}{V_*}\,\frac{s_*}{\Delta_o}\left(1 + \frac{\Delta_o}{R_b}\right)\frac{\rho_1}{\rho_{st}}\left[1 - \left(\frac{\rho_2}{\rho_1} - 1\right)G\right]\frac{s}{s_*} \tag{D2}$$

The relationship between pressure and velocity of a perfect gas, written in a form valid for small velocities, is

$$\frac{p}{p_{st}} = \left[1 - \frac{\gamma - 1}{\gamma + 1}\left(\frac{V}{V_*}\right)^2\right]^{\frac{\gamma}{\gamma-1}} \cong 1 - \frac{\gamma}{\gamma + 1}\left(\frac{V}{V_*}\right)^2 \tag{10}$$

Equations (D2) and (10) are combined to give

$$\frac{p}{p_{st}} = 1 - \left[\nu\,\frac{s_*}{\Delta_o}\left(1 + \frac{\Delta_o}{R_b}\right)\right]^2\left(\frac{s}{s_*}\right)^2 \tag{13}$$

where

$$\nu = \sqrt{\frac{\gamma}{\gamma + 1}} \frac{V_1}{V_*} \frac{\rho_1}{\rho_{st}} \left[1 - \left(\frac{\rho_2}{\rho_1} - 1 \right) G \right]$$

The function ν was determined for gases with $\gamma = 1.0$ and 1.4 as a function of the normal shock-density ratio, ρ_1/ρ_2 (fig. 10).

Sonic Point

Newtonian theory gives for pressure distribution,

$$\frac{p}{p_{st}} = \cos^2 \Phi \tag{D4}$$

The derivative of the pressure distribution with respect to Φ is

$$\frac{d\left(\frac{p}{p_{st}}\right)}{d\Phi} = -2 \sin \Phi \cos \Phi \tag{D5}$$

The pressure gradient at the sonic point on a round corner of radius, r_c, is found by eliminating Φ between equations (D4) and (D5):

$$\frac{d\left(\frac{p}{p_{st}}\right)}{ds} = \frac{d\left(\frac{p}{p_{st}}\right)}{r_c \, d\Phi} = -\frac{2}{r_c} \sqrt{\frac{p_*}{p_{st}} \left(1 - \frac{p_*}{p_{st}} \right)}$$

or, since, generally, $0.5 < p_*/p_{st} < 0.6$,

$$\frac{d\left(\frac{p}{p_{st}}\right)}{d\left(\frac{s}{s_*}\right)} \approx -\frac{s_*}{r_c} \tag{15}$$

Although equation (15) was based on approximate theory, it generally agreed well with available experimental data.

REFERENCES

1. Van Dyke, Milton D.; and Gordon, Helen D.: Supersonic Flow Past a Family of Blunt Axisymmetric Bodies. NASA Rep. R-1, 1959.

2. Kaattari, George E.: Predicted Shock Envelopes About Two Types of Vehicles at Large Angles of Attack. NASA TN D-860, 1961.

3. Kaattari, George E.: Predicted Gas Properties in the Shock Layer Ahead of Capsule-Type Vehicles at Angles of Attack. NASA TN D-1423, 1962.

4. Kaattari, George E.: Shock Envelopes of Blunt Bodies at Large Angles of Attack. NASA TN D-1980, 1963.

5. Traugott, Stephen C.: An Approximate Solution of the Direct Supersonic Blunt-Body Problem for Arbitrary Axisymmetric Shapes. J. Aerospace Sci., vol. 27, no. 5, May 1960, pp. 361-370.

6. Inouye, Mamoru; Marvin, Joseph G.; and Sinclair, A. Richard: Comparison of Experimental and Theoretical Shock Shapes and Pressure Distributions on Flat-Faced Cylinders at Mach 10.5. NASA TN D-4397, 1968.

7. Lawson, Warren A.; McDearmon, R. W.; and Rainey, R. W.: Investigation of the Pressure Distributions on Reentry Nose Shapes at a Mach Number of 3.55. NASA TM X-244, 1960.

8. Newlander, Robert A.; Taylor, Nancy L.; and Pritchard, E. Brian: Pressure Distribution on Two Models of a Project Mercury Capsule for a Mach Number Range of 1.60 to 6.01 and an Angle-of-Attack Range of 0° to 180°. NASA TM X-336, 1961.

NASA-Langley, 1968 —— 1

"The aeronautical and space activities of the United States shall be conducted so as to contribute . . . to the expansion of human knowledge of phenomena in the atmosphere and space. The Administration shall provide for the widest practicable and appropriate dissemination of information concerning its activities and the results thereof."

—NATIONAL AERONAUTICS AND SPACE ACT OF 1958

NASA SCIENTIFIC AND TECHNICAL PUBLICATIONS

TECHNICAL REPORTS: Scientific and technical information considered important, complete, and a lasting contribution to existing knowledge.

TECHNICAL NOTES: Information less broad in scope but nevertheless of importance as a contribution to existing knowledge.

TECHNICAL MEMORANDUMS: Information receiving limited distribution because of preliminary data, security classification, or other reasons.

CONTRACTOR REPORTS: Scientific and technical information generated under a NASA contract or grant and considered an important contribution to existing knowledge.

TECHNICAL TRANSLATIONS: Information published in a foreign language considered to merit NASA distribution in English.

SPECIAL PUBLICATIONS: Information derived from or of value to NASA activities. Publications include conference proceedings, monographs, data compilations, handbooks, sourcebooks, and special bibliographies.

TECHNOLOGY UTILIZATION PUBLICATIONS: Information on technology used by NASA that may be of particular interest in commercial and other non-aerospace applications. Publications include Tech Briefs, Technology Utilization Reports and Notes, and Technology Surveys.

Details on the availability of these publications may be obtained from:

SCIENTIFIC AND TECHNICAL INFORMATION DIVISION

NATIONAL AERONAUTICS AND SPACE ADMINISTRATION

Washington, D.C. 20546